ABSTRACT

RAVI, ANIRUDHH. A Comprehensive Investigation of Integrating Renewable Energy Resources to a Marine Power System – an Indian Research Vessel Case Study. (Under the direction of Dr. Mesut Baran).

With the current awareness on slowing down global warming through global emission control strategies, renewable energy integration in marine power systems is gaining spotlight. Using onboard renewable energy resources, the marine fuel consumption can be optimized to yield emission reduction and fuel cost savings. However, unlike a land power system, maximizing benefits through renewable energy integration in a marine power system is more challenging due to the limited space and weight constraints. Also, for an accurate estimation of the benefits and for a more realistic investigation of the renewable energy integration, an accurate system data has to be used. This work proposes a comprehensive investigation of integrating PV and battery energy storage to a marine vessel by using publicly available real-time datasets to obtain the annual vessel demand and annual PV power generation data. Using the annual demand and PV generation data, the onboard fuel consumption is optimized using PV and battery energy storage through an optimal dispatch scheme that includes a minimum generator operation (MGO) with N-1 safety constraint. Finally, based on the optimal dispatch results, factors that affect the fuel savings are examined and the overall investigation findings are summarized.

A Comprehensive Investigation of Integrating Renewable Energy Resources to a Marine Power System – an Indian Research Vessel Case Study

by
Anirudhh Ravi

A thesis submitted to the Graduate Faculty of
North Carolina State University
in partial fulfillment of the
requirements for the degree of
Master of Science

Electrical Engineering

Raleigh, North Carolina
2021

APPROVED BY:

Dr Mesut Baran Committee Chair	Dr David Lubkeman
Dr Leonard White	

DEDICATION

All glories to Sri Radha Krishna

I dedicate this thesis to my father Mr. Ravi Venugopal, my mother Mrs. Bhuvaneswari Ravi and my mentor Mrs. Utsahamayi Radhika who always believed in me and guided me through the path towards success

BIOGRAPHY

Being fascinated by the importance of electrical energy in everyday life, right from school, Anirudhh Ravi has a zeal towards electrical engineering. The fact that the supply of this important form of energy is monitored and controlled by power system engineers, galvanized his passion towards the field of electrical power systems engineering and motivated him to pursue undergraduate studies in electrical engineering. With his passion, he captured every learning opportunity and his interest towards power systems research gradually developed as he started working on microgrids and energy storage systems as an undergraduate student researcher. With his goal of gaining more knowledge and expertise in the field of power systems, he started pursuing graduate studies in electric power systems. While working on his graduate coursework, he was presented with an opportunity of investigating the integration of renewable energy resources to an Indian research vessel. Since renewable integration in marine power systems is a relatively new research area, he saw this as an exciting opportunity and started working on the project under the supervision of Dr Mesut Baran. Being passionate about power system research, Anirudhh Ravi aims to continue his career in power systems.

ACKNOWLEDGMENTS

I would like to thank all my professors and mentors who invested their time and effort in training me to become a power system engineer. I would like to extend a special thanks to my advisor Dr Mesut Baran for being my advisor, and for being kind and supportive throughout the course of the project. It was a pleasure working with Dr Baran and I look forward for an opportunity to collaborate with him again.

I would like to thank Dr Leonard White and Dr David Lubkeman for being my committee members. Dr White's practical experience with diesel generators was very helpful in answering some of the key questions behind the fuel consumption characteristics of diesel generators. I also would like to thank Mr. Valliappan Muthukaruppan, a doctoral student working under the supervision of Dr Baran, for educating me on the basics of mathematical optimization techniques and the use of MATLAB-YALMIP to solve optimization problems.

Finally, to all those who prayed for my success, I would like to extend my warmest gratitude to you, and you will always be in my memory.

TABLE OF CONTENTS

LIST OF TABLES

LIST OF FIGURES

CHAPTER 1. INTRODUCTION

Similar to land power systems where use of conventional energy resources like coal and oil lead to emission of pollutants to the atmosphere, in marine power systems, diesel engines that are typically used for propulsion and auxiliary power supply, emit pollutants such as carbon dioxide, sulphur dioxide etc. to the atmosphere [1]. According to a study performed by the international maritime organization (IMO), global greenhouse gas emissions due to shipping is about 1,076 million tonnes [2]. The pollutants emitted due to the combustion of diesel fuel cause serious health problems such as heart disease, lung disease and even early mortality [3]. Due to the serious health concerns caused by inhaling these pollutants, recently, measures such as compliance with the energy efficiency performance levels and improvising the energy efficiency through operational means such as speed optimization and weather routing, have been imposed by the IMO to curtail the global marine emissions [4].

With the aim of optimizing the fuel consumption and curbing emissions, modern ships are employing an onboard integrated power system utilizing efficient propulsion systems and ultra-low sulphur diesel fuel for diesel engines [5]. Also, in an integrated power system, the system reliability is improved through the interconnection of generation sources with propulsion and auxiliary loads [6], [7]. Additionally, renewable energy resources such as solar PV and hydrogen fuel along with storage devices such as batteries and super capacitors are being interconnected to the onboard power system to optimize fuel consumption and to improve the system reliability and power quality [8]–[11]. With renewable energy integration, the concept of onboard DC power system is also gaining popularity due to its significant advantages in easy integration of renewable energy resources and optimizing the fuel consumption of diesel generators through variable speed operation [12]–[16]. In [17], a DC platform supply vessel with solar PV and battery energy storage

was modelled to perform real-time optimal load scheduling, whose objective is to minimize the specific fuel oil consumption (SFOC), and the response of the proposed optimal load scheduling algorithm was studied under different generation and load contingencies conditions. The study illustrated the reduction in SFOC during each operating condition that was simulated but did not consider the actual power demand profile of the vessel to realistically evaluate the SFOC savings and did not evaluate the economic and environmental benefits due to the SFOC optimization. Also, the battery sizing neglects the actual power demand profile of the vessel thereby leading to an unrealistic sizing estimate [18], [19].

To ensure efficient operation and compliance with the IMO energy efficiency and emission standards, management of the onboard resources is also important. Diesel generators have their optimal SFOC region at higher power levels, typically, greater than 60% of their nominal rating [20]. However, due to the highly dynamic nature of the propulsion demand, more than required number of generators must stay online, called as the minimum generator operation (MGO), to quickly respond under generation contingencies or sudden demand changes for prevention of partial or complete loss of load [21], [22]. The minimum number of online generators or the MGO is determined based on the N-1 contingency or safety and this MGO based N-1 safety is required, especially, for ships that have dynamic positioning [23]. Therefore, some generators are dispatched to supply a low demand condition which leads to a higher and inefficient fuel consumption. Unlike optimizing the usage of diesel generators through variable speed operation in a DC power system, in an AC power system, which is the common architecture for ships under operation, the diesel generators must maintain a constant synchronous speed, thereby making the optimization process relatively challenging [24]. To add a degree of freedom in the control of diesel generators for

optimizing their fuel consumption in a marine AC power system, storage devices like batteries can be used.

With the renewable energy integration gaining attention in marine power systems for fuel and emission savings, it is essential to properly size the renewable energy systems to ensure a good investment. Unlike land power systems where a standalone PV system is sized based on the load profile and the power requirement at the point of interconnection [19], in a marine power system, the sizing is primarily done based on the available surface area for installation. The onboard battery energy storage system (BESS) is sized based on the power demand profile of the vessel and its application (for example, to improve power reliability, optimize the usage of diesel generators or provide interim power until backup generator synchronizes) [25], [26]. As stated earlier, to ensure system reliability, it is necessary to use the actual demand profile characteristics of the vessel while sizing a hybrid marine power system comprising of diesel generations and renewable energy resources. In [27], a real time navigation route of a shipping vessel was considered to obtain its demand profile under various operating conditions, and a novel multi-objective particle swarm optimization (PSO) was used to determine the optimal sizes of diesel generator, solar PV and battery energy storage based on the load profile characteristics to ensure reliability, and to minimize the overall system costs and emissions. The PV power was estimated using the irradiation data from the cities or ports that the vessel passes along its voyage, but the distance between the data sources was not considered leading to an estimation error that indirectly affects the accuracy in sizing the onboard generation resources. This shortcoming was addressed in [28], where the distance between the data sources were accounted and the solar irradiation and temperature was calculated using a weighted average approach. Also, the study performed a techno-economic assessment of integrating PV to the existing shipboard power system and

performed an environmental performance analysis. In [29], the BESS capacity for a naval vessel was determined based on the fuel savings achieved through generator scheduling with N-1 safety and different power capacities. Although it considers the N-1 safety while scheduling the generators, it does not consider a real-time demand profile nor accounts the impacts of added weight on the overall fuel consumption due to the proposed storage integration.

Since control of energy storage and onboard diesel generators is critical in achieving reduced fuel consumption, in some works optimal generation scheduling, or optimal unit commitment schemes have been proposed. An efficient power management strategy using a decentralized model predictive control (MPC) strategy that considers the optimal SFOC region for the onboard diesel generators and the safe SOC operating region of batteries was proposed in [34]. A mixed integer linear programming (MILP) based energy management system (EMS) for vessels with electric propulsion powered by diesel engines was proposed in [31]. Similar works with the sole focus of achieving optimal control of onboard resources were found [32]–[35]. Although these works provide the optimal dispatch results, among which some of them use a real-time data and quantify the achieved fuel savings, they consider a pre-defined capacity of storage resources and did not discuss about optimal sizing or the techno-economics of the proposed system.

Based on the knowledge gained through the literature review, it has been found that for a realistic investigation of integrating renewable energy resources to existing marine power systems, real-time datasets must be used to schedule the onboard resources. For vessels that utilize dynamic positioning, the scheduling must also include the minimum generator operation (MGO) based on N-1 safety to ensure reliability and quick response to demand changes. While a few articles use real-time datasets to quantify the fuel savings achieved by their proposed system, to the best of the author's knowledge, a comprehensive study that discusses optimal scheduling of diesel generators

with the N-1 safety by using a real-time data to optimize the diesel fuel consumption, along with sizing of onboard renewable generation or storage resources and a corresponding techno-economic evaluation of the proposed system through quantification of the fuel and emission savings was not present.

Therefore, this work aims to provide a comprehensive realistic investigation of integrating the renewable energy resources to an existing marine power system whose components are listed as follows –

1. Analyse the actual demand profile of an actual vessel and identify the scope of solar PV and battery energy storage integration.
2. Estimate the power produced by the onboard PV based on the proposed accurate irradiation and temperature data extraction technique.
3. Sizing of battery energy storage system based on optimal scheduling of diesel generators with N-1 contingency using the demand profile of the vessel and the fuel consumption characteristic of the diesel generators.
4. Study the impact of different factors that affect the benefits of onboard storage integration.
5. Compare the emissions of the baseline case with renewable integration comprising of solar PV and battery energy storage individually.
6. Evaluate the economics of the proposed system.

To test and demonstrate the performance of the schemes developed, a case study based on an actual ship was adopted. The ship considered is an Indian research vessel (R/V) – Sagar Tara, operated by the National Institute of Ocean Technology (NIOT). The case study objective is to individually investigate the benefits and feasibility of integrating solar PV and energy storage on this vessel and to submit the investigation results and the initial design to NIOT.

CHAPTER 2. ESTIMATING THE LOAD PROFILE OF A SHIP

Since the proposed work aims at studying the operational profile of an Indian research vessel (R/V Sagar Tara) to investigate the opportunity for integration of solar PV and battery energy storage, performing the investigation based on a real operational profile shall yield realistic results that can be applied for real-time implementation of the proposed system. This section discusses the data extraction and the estimation of the annual demand of the vessel.

2.1. Estimating the annual real power demand of the vessel

The annual real power demand of the vessel is estimated based on the operational profile of the vessel that comprises of parameters such as speed, coordinates and the operational status [22] that are part of the automatic identification system (AIS) data structure. Since, the data for the specific vessel under study was not available, the data for a similar research vessel that operates on the USWC – US West Coast was obtained from the MarineCadastre – U.S. National Oceanic and Atmospheric Administration AIS data repository using the maritime mobile service identity (MMSI) which is unique to every vessel. Therefore, this study assumes the case of operating the vessel under study in the US west coast. Also, since 2020 was affected by the coronavirus pandemic and during 2019, the chosen vessel had few movements, the AIS data from 2018 was used for the case study.

The extracted speed data from the AIS data repository, as shown in Figure 1, was normalized based on the second peak value, as shown in Figure 2, since the first peak occurred at an instant and this was assumed to be a surge. The normalized speed data was used to get the speed profile of the Indian research vessel based on the maximum recorded speed provided by the vessel operator, as shown in Figure 3.

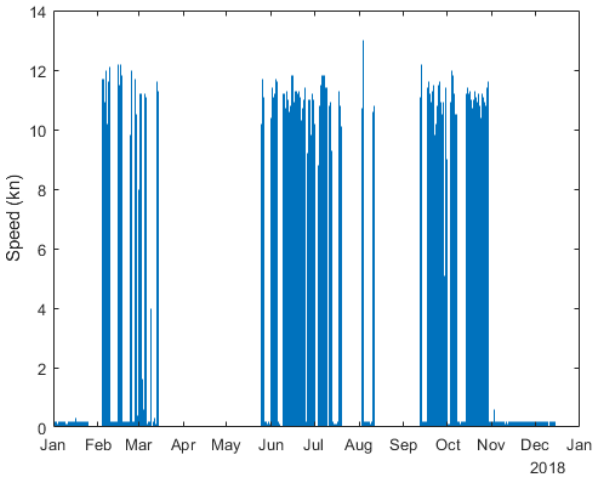

Figure 1. Annual speed profile of the chosen US vessel.

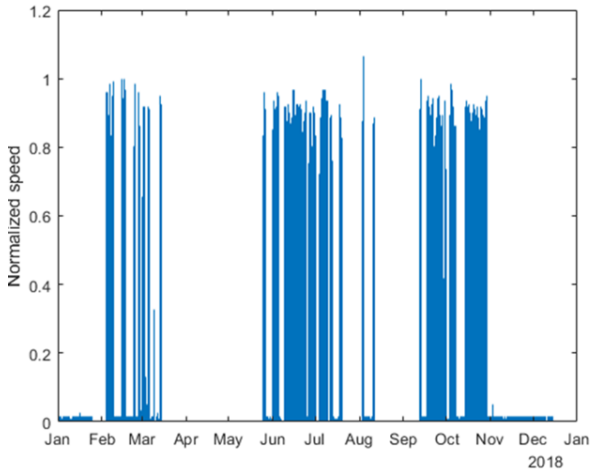

Figure 2. Normalized annual speed profile of the chosen US vessel.

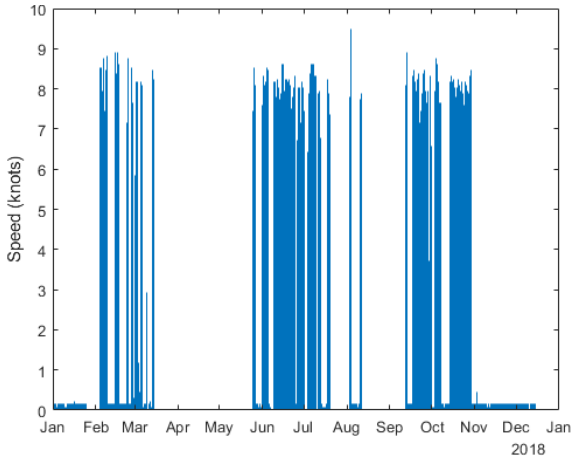

Figure 3. Annual speed profile of the Indian research vessel.

Now that the speed profile of the vessel is estimated, the demand profile of the vessel can be estimated based on the operating mode of the vessel. Under anchored or docked conditions, it is assumed that the total demand only comprises of auxiliary loads, whereas under cruising or maneuvering modes, the total demand is a combination of the propulsion demand and the auxiliary demand. To estimate the propulsion demand of the vessel based on the speed profile, it is assumed that the azimuth thrusters are operated under cruising mode and the bow thrusters are operated under maneuvering mode. Also, for simplicity, it is assumed that the thruster speed is the same as

the propeller speed, thereby, ignoring drivetrain losses. Based on these assumptions, the real power versus ship speed relationship is obtained by modelling the relationships between the ship speed and thruster speed, and the thruster speed and propeller torque.

Starting with the ship speed and thruster speed relationship, the thruster speed is the speed at which the azimuth thrusters or the bow thrusters operate. As mentioned before, it has been assumed that the thruster speed is the same of the propeller speed. The propeller speed need not always be the same as the ship speed because while the ship is in motion, it experiences resistances such as viscous resistance, air resistance and wave-making resistance. Therefore, to plot the relationship between the ship speed and the thruster or propeller speed, a propeller mathematical model from [36] was used. Here, for a known propeller diameter, the propeller speed was iteratively varied and during each iteration, the calculated ship speed was noted. This iterative process was stopped when the ship speed reached the maximum possible value. The obtained relationship was then normalized and plotted as shown in Figure 4.

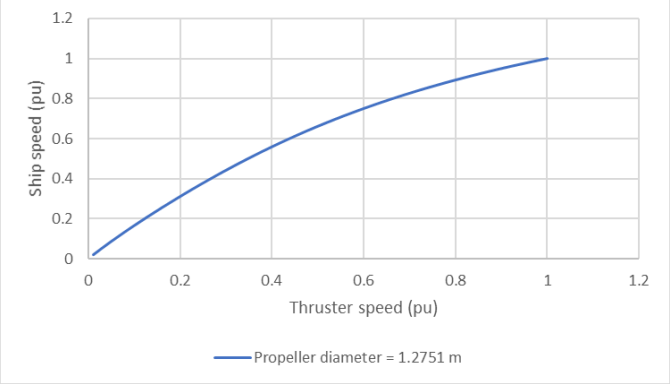

Figure 4. Normalized ship speed versus thruster (or propeller) speed.

Similarly, using the propeller speed, the propeller torque was calculated by the mathematical model used in [36] and the relationship between them was normalized and plotted as shown in Figure 5. Based on the propeller torque, the mechanical power delivered by the thrusters was calculated using equation (1) and the relationship is plotted as shown in Figure 6.

$$P_m = T \times \omega \quad (1)$$

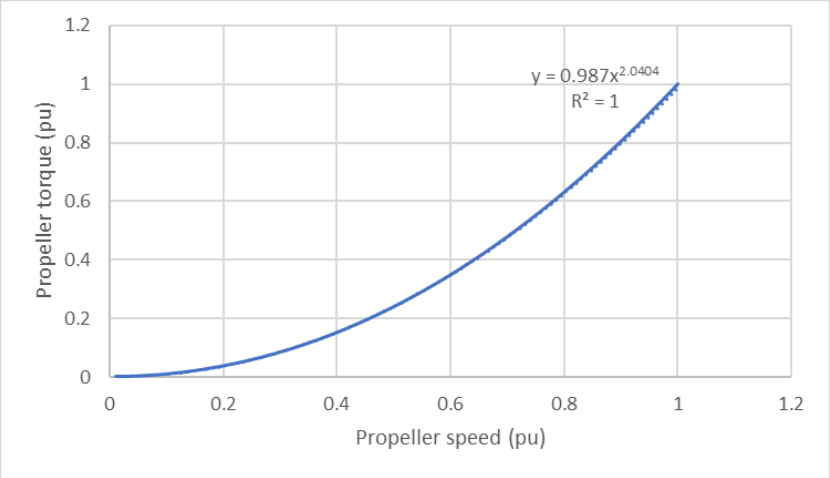

Figure 5. Normalized propeller torque versus speed.

The obtained relationship between the mechanical power delivered by the thruster and the propeller speed can be mathematically verified as shown in equation (3).

$$T \propto \omega^2 \quad (2)$$

$$P_m \propto T \times \omega \rightarrow P_m \propto \omega^3 \quad (3)$$

Where,

P_m = Mechanical power delivered by the thruster to the propeller in pu

T = Propeller torque in pu

ω = Propeller speed in pu

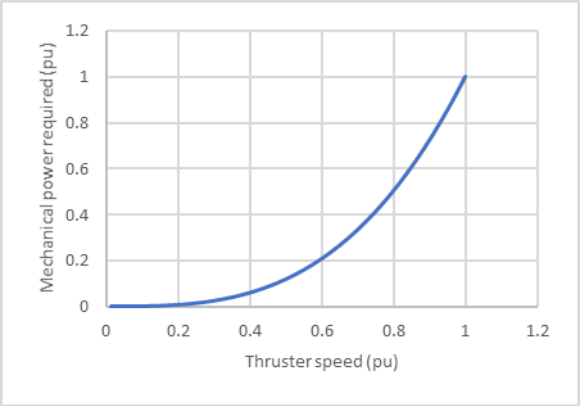

Figure 6. Normalized mechanical power delivered by thruster versus propeller speed.

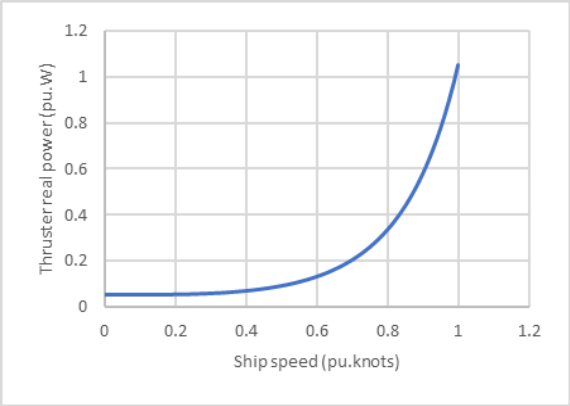

Figure 7. Normalized real power consumed by thruster versus ship speed.

Finally, using the mechanical power versus thruster speed relationship, the real power consumption of the thrusters was obtained as shown in Figure 7 by assuming a 95% motor efficiency. This relationship shows that the real power demand profile of the vessel can be estimated if the speed profile of the vessel, as shown in Figure 3, is known. This real power demand profile estimation is shown in Figure 8 for the vessel considered in this study. The constant demand periods correspond to the anchor/docked mode of the ship, where the demand profile assumes a constant auxiliary power consumption.

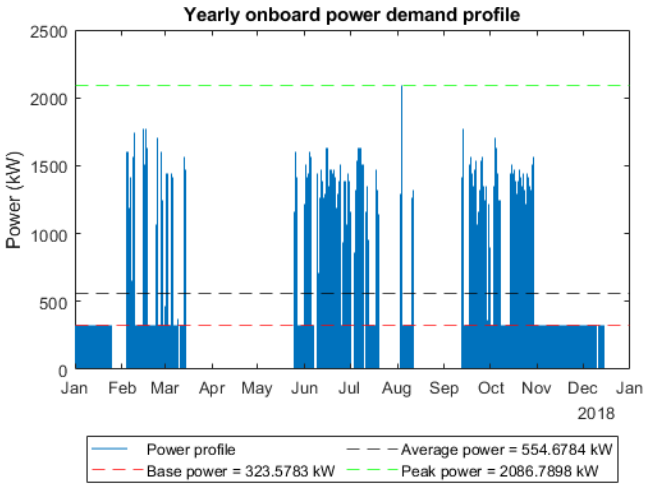

Figure 8. Annual real power demand profile.

Based on the distribution of operating conditions of the ship, as shown in Figure 9, it can be seen that the ship is stationary i.e., uses only auxiliary power (323 kW) for about 45% of the entire year. This condition corresponds to an inefficient operation of the diesel generators, leading to formation of soot and increased maintenance service frequency. Therefore, integration of energy storage may lead to potential fuel savings by operating the diesel generators at optimal conditions. Solar PV may also be used for direct demand supply to reduce the overall fuel consumption and the yearly emissions.

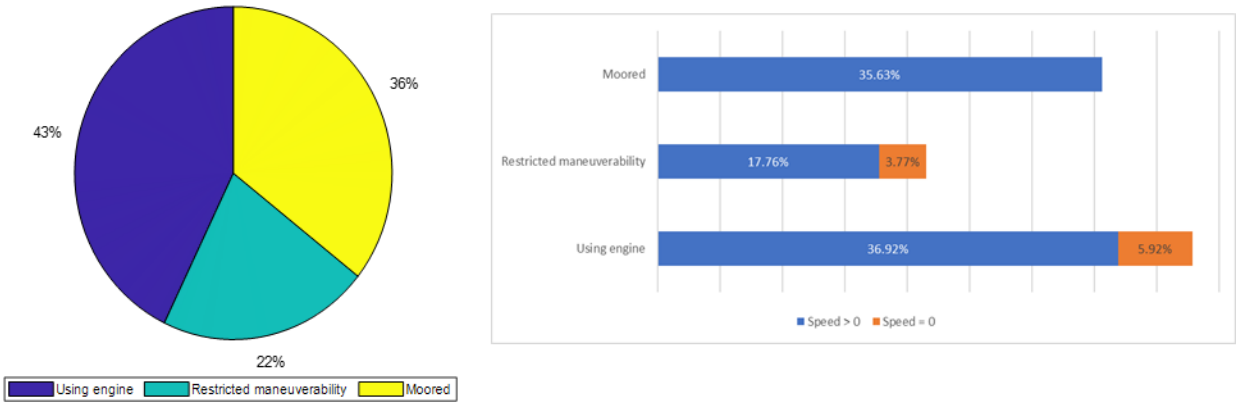

Figure 9. Distribution of operating conditions.

2.2. Handling inconsistencies in data

From the annual real power demand profile, as shown in Figure 8, it can be seen that the data is not consistent, that is, there are missing timestamps. Therefore, for a uniform ship demand profile, the estimated power data is averaged every hour and the data for a missing timestamp is filled based on the previous operating mode and by inspecting the movement plot. For example, if there is a missing demand data while the ship is docked, then the missing data is assumed to be 323 kW, which is the assumed auxiliary power value.

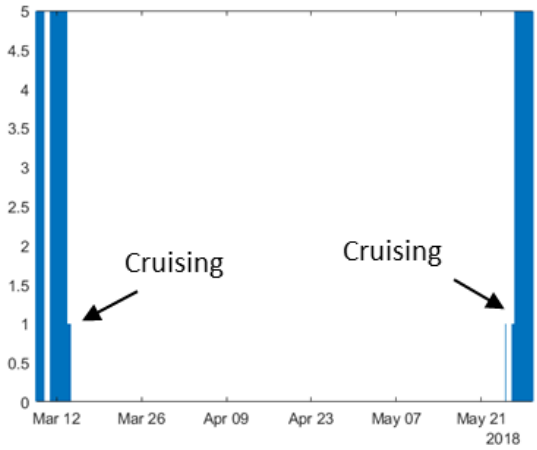

Figure 10. Handling missing timestamps.

For longer missing periods, like March 12 – May 21, as shown in Figure 10, the movement plots are used to handle the data inconsistency. As shown in Figure 10, it can be seen that the missing time stamps are between two cruising operating modes and from the movement plots, as shown in Figure 11 and Figure 12, the last recorded location of the ship for March is 29.5 °N, -116.7 °W and the first recorded location for May is 31.1 °N, -116.5 °W. Based on this position data, it has been assumed that the ship was stationed at 29.5 °N, -116.7 °W consuming only auxiliary power over the rest of March, the entire month of April and started moving north just before May 21, consuming the cruising power recorded at May 21, as illustrated in Figure 13.

Similarly, the missing demand data was filled and since the timestamps are inconsistent, where the interval between two consecutive timestamps is not the same, an hourly rolling average is applied to the yearly demand data to get an 8760 data as shown in Figure 14.

Figure 11. Movement plot for March 2018.

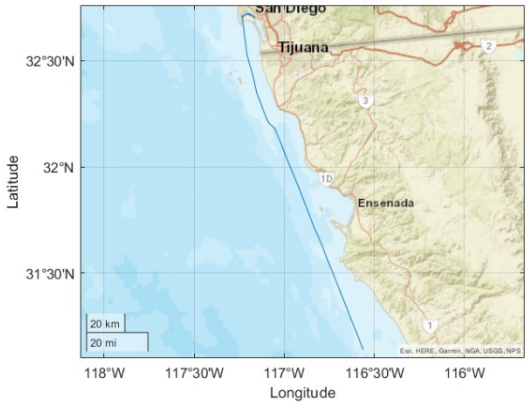

Figure 12. Movement plot for May 2018.

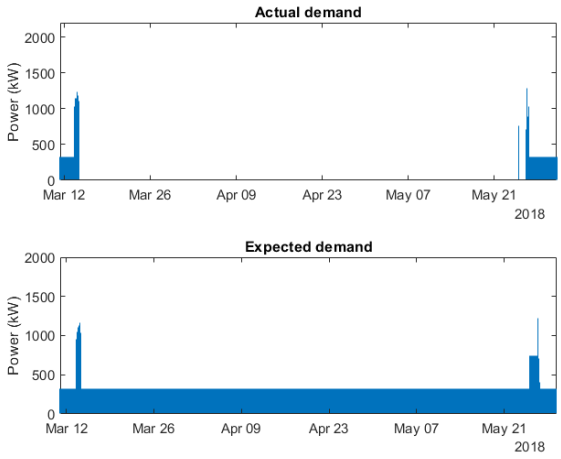

Figure 13. Actual and expected demand for March – May 2018.

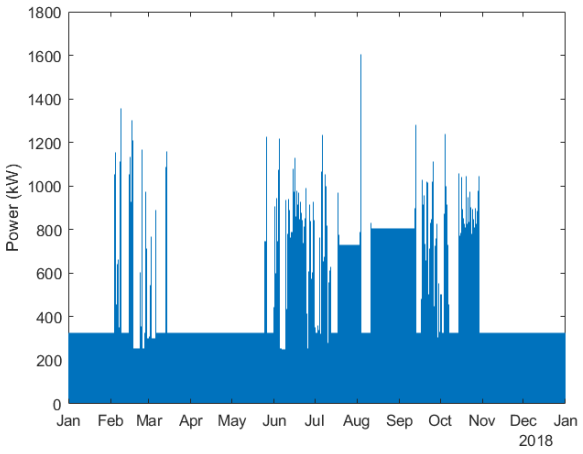

Figure 14. 8760 demand plot.

CHAPTER 3. BATTERY ENERGY STORAGE SYSTEM (BESS) INTEGRATION

As mentioned earlier, under moored conditions, typically, vessels have only auxiliary loads online, therefore, the total system demand is usually much lower than the total generation capacity of a vessel. Using diesel generators to supply this low demand not only results in an inefficient operating condition but also leads to formation of soot that triggers regular maintenance of the generators, leading to increased maintenance expenditure. Using a battery energy storage device, the total system demand under moored conditions can be increased by charging the battery, thereby increasing the loading of generators, and under cruising or maneuvering modes, the battery can be discharged to save diesel fuel consumption.

Based on the literature review, it was found that the minimum generator operation (MGO) with N-1 safety is essential for vessels with dynamic positioning operations [23]. While some papers discussed the importance of this safety, to the best of the author's knowledge, they did not include the safety as a constraint in their optimal scheduling schemes [31]. Since the vessel under study utilizes dynamic positioning to maintain its position while taking oceanographic and hydrographic measurements, the optimal scheduling scheme includes the N-1 safety constraint. This optimal scheduling process starts with an initial assumption of the battery capacity. This initial capacity is then incremented until a maximum capacity value is reached, and the optimal scheduling process is performed for each battery capacity. Here, the maximum capacity is estimated based on the maximum allowable additional loading of the vessel, which is about 48 tonnes. Also, as mentioned before, for a realistic dispatch, the real time data obtained in the previous section is used by the optimal scheduling scheme.

3.1. Optimal scheduling of diesel generators with battery energy storage

The objective of this proposed optimal scheduling approach is to minimize the diesel fuel consumption using battery energy storage, therefore, a fuel consumption characteristic of the diesel generators is essential. The fuel consumption chart shown in Figure 15 is adopted for the case study. This characteristic is obatined by using the fuel consumption chart taken from [37]. As the figure shows, it is intuitive that the diesel fuel consumption increases with increasing loading.

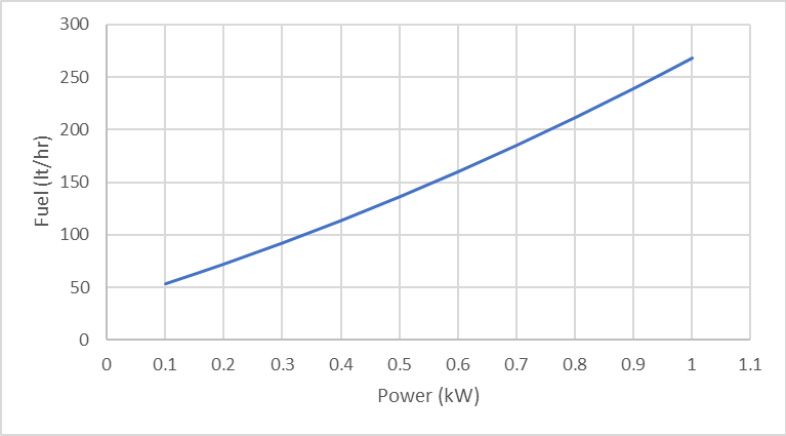

Figure 15. Fuel consumption characteristic.

Using the figure, a quadratic curve fit equation is obtained using Excel that would relate the diesel fuel consumption with the loading of the generator and is shown below.

$$\text{Fuel} = 7 \times 10^{-5} P_{dg}^2 + 0.178 P_{dg} + 35.961 \quad (4)$$

Where,

Fuel = Diesel fuel consumption by the generator (lt/hr)

P_{dg} = Loading of the generator (kW)

Based on equation (8) it can be seen that, since the quadratic coefficient is low, the fuel consumption is more linearly related with the diesel generators. However, this work does not neglect the quadratic coefficient since it was observed that the savings in fuel consumption

achieved by the optimal scheduling algorithm is signifcantly affected by the accuracy of the curve fit.

3.1.1. Objective function

Since the objective of the optimal scheduling problem is to reduce the fuel consumption of the diesel generators, the objective function (J) for the optimization problem can be written as shown below.

$$J = \min \sum_{t=1}^{T} \left(\sum_{n=1}^{N_{DG}} \text{fuel}(n)_t \right) \quad (5)$$

Where,

$\text{fuel}(n)_t$ = Diesel fuel consumption for n^{th} diesel generator at time t (lt/hr)

N_{DG} = Total number of diesel generators

T = Time period of the optimization horizon (hr)

Note that the proposed work aims to study the benefits of battery storage separately from the PV. Therefore, this optimal dispatch scheme comprises of the onboard DGs and the battery storage.

3.1.2. Constraints

Based on the fuel equation, as shown in equation (4), it can be seen that when a DG is online and does not generate any power, it consumes some fuel to stay online. Therefore, while solving the optimization problem it has to be ensured that the fuel is only calculated for DGs that are online. This can be ensured by introducing a DG status variable, however, adding a DG status variable to the existing quadratic fuel consumption equation not only makes the objective function complicated, but also results in limited availability of computational solvers since it will then become a polynomial objective function. To handle this issue, since the vessel under study has 3

DGs, the third DG is set to be online only for high demands, therefore the summation for total fuel consumption at a given time can be ensured to only include the DGs that are online.

In any power system, power balance is critical to ensure system security and power quality. Therefore, a power balance constraint is defined as shown below. Separate terms were used for charging and discharging powers of battery to enable defining charging and discharging efficiencies.

$$\sum_{n=1}^{N_{DG}} P_{DG(n)_t} = P_{d_t} - P_{b-dis_t} - P_{b-chg_t} \quad (6)$$

Where,

$P_{DG(n)_t}$ = Power generated by n^{th} DG at time t (decision variable)

P_{d_t} = System demand at time t (time varying)

P_{b-dis_t} = Battery discharge power at time t (decision variable)

P_{b-chg_t} = Battery charge power at time t (decision variable)

Since the power generated by the DG has to be a finite positive value, a DG power constraint is defined as shown below. A DG status control variable is used to ensure that the DG power constraint is only applied to DGs that are online. Also, since the DGs in the vessel under study have the same rating, the rated power (P_{DG}^{mx}) is the same for all the DG units.

$$0 \leq P_{DG(n)_t} \leq U_{DG\,(n)_t} \times P_{DG}^{mx} \quad (7)$$

Where,

$U_{DG\,(n)_t}$ = Status of n^{th} DG at time t (control variable)

P_{DG}^{mx} = Rated power of the DG (constant)

Since a marine power system is highly dynamic in nature, as mentioned earlier, more than required number of generators must stay online, especially for vessels like the vessel under study with dynamic positioning, to quickly respond to any generation or demand contingencies and this safety precaution is termed as the MGO based N-1 safety. As the proposed optimization approach considers the N-1 safety while scheduling the DGs, the MGO based N-1 safety is determined.

For the vessel under study, the generation system comprises of three 950 kW diesel generators. The number of online DGs based on the N-1 safety is calculated using (8) and (9) and the generator combinations based on the N-1 safety are shown in Table 1. As shown in (8), the safe load factor is calculated based on the condition where the largest generator of the system goes offline for any reason. Under such a condition, there should be a enough generation capacity to supply the continuously the system demand until a backup or another generational source comes online (start-up time). As shown in Table 1, combo 1 is not safe for operation since under an event of a generator loss, the maximum load that can be supplied during the start-up time of a backup or another generator is zero. Combo 2 is safe for operation as long as the demand is less than 950 kW, since under a generator failure condition, the other online generator can continue to supply a maximum demand of 950 kW. Similarly, combo 3 is safe for operation as long as the demand is less than 1,900 kW.

$$LF_{safe} = \frac{P_{G-total} - P_{trip}}{P_{G-total}} \times 100 \quad (8)$$

$$P_d^{mx} \leq LF_{safe} \times P_{G-total} \quad (9)$$

Where,

LF_{safe} = Maximum load factor for safe operation (%)

$P_{G-total}$ = Total generation capacity (MW)

P_{trip} = Power rating of the largest generator (MW)

Table 1. Generator combinations based on N-1 safety.

Combo #	Generator combination	Total generation capacity ($P_{G\text{-}total}$)	Safe load factor, Lf_{safe} (%)	Suppliable load after one generator loss ($MW_{s\ (max)}$)	Maximum demand for safe operation ,P_d^{mx} (MW)
1	DG_1	0.95	0	0	0
2	$DG_1 + DG_2$	1.90	50	0.95	0.95
3	$DG_1 + DG_2 + DG_3$	2.85	66.67	1.90	1.90

Therefore, based on the N-1 safety calculations, the MGO based N-1 safety constraint is defined as shown below.

$$N_{DG_t}(P_{d_t}) = \begin{cases} 2, & P_{d_t} \leq 950\ kW \\ 3, & P_{d_t} > 950\ kW \end{cases} \quad (10)$$

Where,

$N_{DG_t}(P_{d_t})$ = Number of DGs online at time t, defined as a function of the total system demand at time t

P_d^{mx} = Maximum (utmost – not inclusive) demand for safe operation of N DGs

Note that the constraint uses the vessel demand (exclusive of the battery storage) rather than the total system demand (that includes the battery power) because, in this application, battery is used as a separate resource to optimize the fuel consumption for the vessel under study and cannot be considered as a 'generator' therefore, cannot be used in the MGO with N-1 safety criteria. Intuitively, this ensures reliability since if the battery system suddenly goes offline, sufficient number of diesel generators are still online to continuously supply the system demand.

Since the charging and the discharging power for a battery has to be within a definite range to protect the battery from overheating and to ensure efficient operation, battery charge and discharge power constraints are defined as shown in below where The maximum charging and discharging powers are determined based on a 1-C rate operation. As shown below, a battery status control variable (u_{b-chg_t}) is also used to differentiate between charging and discharging modes. For example, if the battery is charging, then the battery discharging power variable (P_{b-dis_t}) is set to zero.

$$0 \leq P_{b-dis_t} \leq (1 - u_{b-chg_t}) \times P_b^{mx} \quad (11)$$

$$u_{b-chg_t} \times P_b^{mn} \leq P_{b-chg_t} \leq 0 \quad (12)$$

Where,

u_{b-chg_t} = Charging status of the battery at time t (control variable)

P_b^{mx} = Maximum battery power or maximum discharging power (constant) = $\frac{E_{rated}^{batt}}{1\ hr}$

P_b^{mn} = Minimum battery power or maximum charging power (constant) = $-\frac{E_{rated}^{batt}}{1\ hr}$

E_{rated}^{batt} = Energy rating of the battery (constant for a given 1 year optimization iteration)

In addition to the charge and discharge power limits, state of charge (SOC) limits should also be defined for a battery to ensure safe and efficient operation. Therefore, an SOC constraint is defined as shown below.

$$SOC_{min} \leq (SOC)_t \leq SOC_{max} \quad (13)$$

Where,

$(SOC)_t$ = SOC at time t (calculated)

SOC_{min} and SOC_{max} = Minimum and Maximum SOC limits (assumed to be 10% and 100% respectively)

Considering the charge and discharge efficiencies of the battery, the SOC is calculated using coulomb counting method as –

$$(SOC)_t = (SOC)_{t-1} - \frac{(P_{b-dis})_t}{E_{batt}^{rated} \times \eta_d}\Delta T - \frac{(P_{b-chg})_t \times \eta_c}{E_{batt}^{rated}}\Delta T \quad (14)$$

Where,

η_d = Discharge efficiency of the battery (constant) = $\sqrt{\eta_{RTE}}$

η_c = Charge efficiency of the battery (constant) = $\sqrt{\eta_{RTE}}$

η_{RTE} = Round trip efficiency of the battery (constant)

CHAPTER 4. PV INTEGRATION

The capacity of a marine PV system depends on the surface area available for PV installation. This area has to be a non-commercial area and away from the ship rails to prevent regular splashing of salt water on the panel surface. Therefore, the proposed system assumes that the PV panels are installed on a raised surface above the deck. The total available surface area for the PV installation in the vessel under study is 200 square meters.

For the proposed system, marine grade PV panels were chosen to have water-resistant and corrosion-resistant frames, and a good wind withstand rating. Due to these added features, marine grade PV panels tend to be expensive than a terrestrial PV panel. It has been identified that, typically, the $/W cost of marine PV panels is about 1.2 – 1.5 times the $/W cost of terrestrial PV panels depending on the total wattage of the panel. A PV panel was chosen based on the lowest $/W cost and the maximum number of PV panels is calculated to be about 203 based on the available surface area estimate of 200 m^2 and the panel dimensions (per panel area is 0.9849 m^2). Finally, based on the maximum number of panels and the panel rating of 165 W, the maximum possible PV capacity is estimated to be about 33 kW. Alternatively, the maximum PV power can also be estimated based on the panel efficiency, which is, 167 W/m^2.

Table 1 lists the key parameters of the chosen PV panel, and the cost summary of the proposed PV system is provided in Table 2.

Table 2. Key specifications of the chosen PV panel.

Manufacturer	**Nature power**
Maximum power	165 W
Vmpp	18.94 V
Impp	8.72 A
Maximum system voltage	1000 V
Panel dimensions	26.3 x 1.4 x 57.8 inches
Weight	24.6 lbs

Table 3. Summary of costs - PV system.

Component	**Quantity**	**Per item cost**	**Total cost**
PV panel – 165 W	203	$549.99	$111,647
PV inverter – 30 kVA, corrosion-resistant NEMA 4X enclosure	1	$3,000	$3,000
Transformer – 480/690 Vac, 30 kVA	1	$749	$749
Additional rust and corrosion resistant support rods – 0.1 m	50	$0.56	$28
Total			$115,424

4.1. Estimating the annual irradiation and ambient temperature

To estimate the impact of solar PV integration on fuel consumption and emissions, it is necessary to estimate the power generated by the proposed solar PV system. Unlike terrestrial solar PV systems, the power produced by a marine PV system depends on the route taken by the vessel and the weather conditions. Therefore, it is more challenging to estimate the power produced by a marine PV system since using the irradiation and ambient temperature data for a single latitude and longitude coordinate would not yield accurate results.

Existing methods for estimating solar PV power production use the solar irradiation and the temperature data measured at nearby ports that a vessel passes by along its voyage [25] or since the distance between the ports are not always equal, apply a weighted average approach for better accuracy, where the ratio of the distance between two measurement points to the total distance of the entire voyage is used as the weight [24]. These methods may be valid for vessels that move close to the measurement points, that is, close to harbors or ports, but for vessels that typically journey away from the coastline, these existing methods may not be suitable for estimating the power produced by the solar panels.

Since research vessels are often stationed away from the coastline for hydrographic or oceanographic studies, this work uses a different technique to get the solar irradiation and the ambient temperature data, as illustrated in Figure 16. Here, the latitude and the longitude coordinates for a given timestamp is taken from the vessel's AIS data and the great circle distance between the vessel's location and all the available data sources is calculated to find the closest available data source. Then, the global horizontal irradiation (GHI) and the ambient temperature data from the closest available data source for a given timestamp is extracted. Figure 17 illustrates the working of the proposed data extraction technique where the data source closest to the ship's actual location is used to get the irradiation and temperature data. Also, from Figure 18, it can be seen that the distance between the actual ship location and the data source used by the proposed data extraction technique is predominantly less than 1.3 nautical miles.

It has to be noted that, although, based on the plot shown in Figure 17 it may seem that the closest data point chosen by the extraction is irregular, this however depends on the availability of the closest data source. It has been observed that based on the ship's location and the time, the closest available data source is either near the coastline (case A in the zoomed plot) or near the

vessel (case B in the zoomed plot). Although this method is computationally intensive, it uses the closest available data source thereby yielding accurate results when estimating the PV power, which is essential for realistic investigative studies.

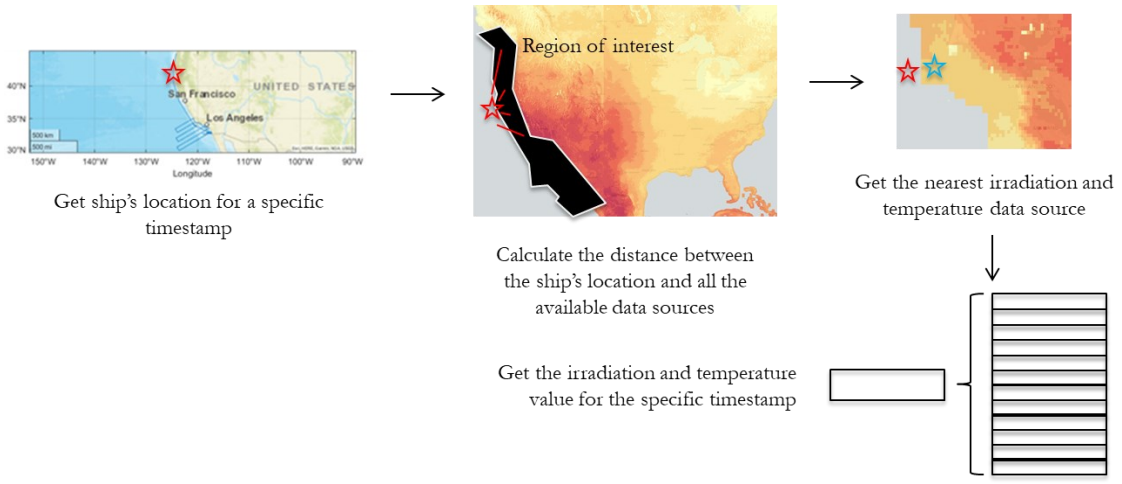

Figure 16. Irradiation and temperature data extraction.

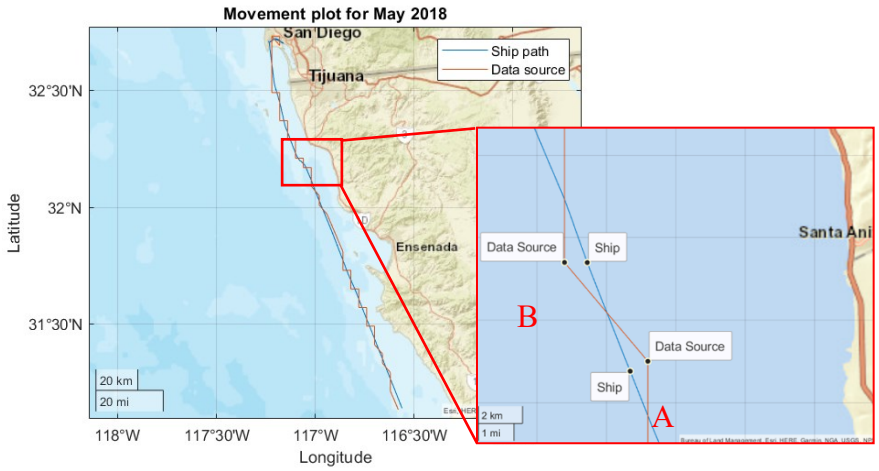

Figure 17. Data source locations and ship movement.

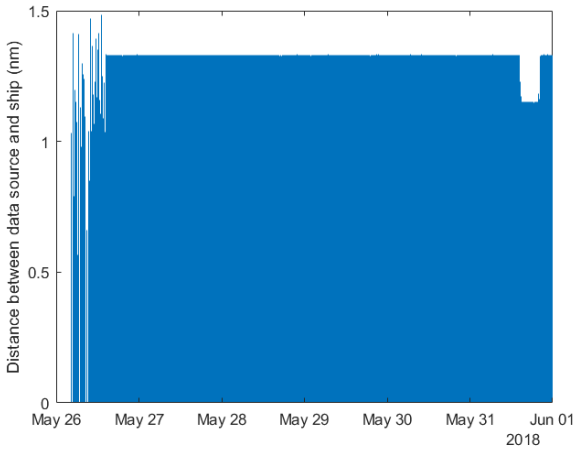

Figure 18. Distance (in nautical miles) between the data source and the actual ship location.

4.2. Estimating the annual PV power production

Based on the estimated maximum PV capacity of 33 kW and using the estimated GHI (or solar insolation) and the ambient temperature from the previous section, the PV power production with the derating factors can be estimated as shown below.

$$P_{PV} = P_{mp}^{rated} \times D_{total} \times S \quad (15)$$

Where,

P_{PV} = Power produced by the PV panel (kW)

P_{mp}^{rated} = Maximum power rating of the PV panel (kW)

D_{total} = Total derating factor = $D_{mismatch} \times D_{inv} \times D_{temp}$

S = solar insolation (kWh/m^2)

Furthermore, the total derating factor is calculated as a combination of different derating factors as shown below.

$$D_{total} = D_{mismatch} \times D_{inv} \times D_{temp} \quad (16)$$

Where,

$D_{mismatch}$ = Derating factor due to PV mismatch (assumed to be 97%)

D_{inv} = Inverter derating factor (assumed to be 95%)

D_{temp} = Temperature derating factor = $\left(1 - \alpha_P(T_{cell} - 25°C)\right)$

Where, α_P = Temperature-power coefficient

T_{cell} = Cell temperature

To estimate the temperature derating facture, the cell temperature is calculated based on the ambient temperature data, estimated using the ship's actual location as described in the previous section, as shown below.

$$T_{cell} = T_{ambient} + \frac{NOCT - 20°C}{0.8} \quad (17)$$

Where, NOCT = Nominal operating cell temperature (assumed to be 50°C)

Figure 19 illustrates the annual PV production calculated using equations (15) – (17), and the impact of the limited surface area for PV installation can be seen from the low annual average value of generated PV power. Note that the missing timestamps were handled similar to the previous section, where, instead of an expected demand value, the expected latitudes and longitudes were used to estimate the irradiation and the ambient temperature.

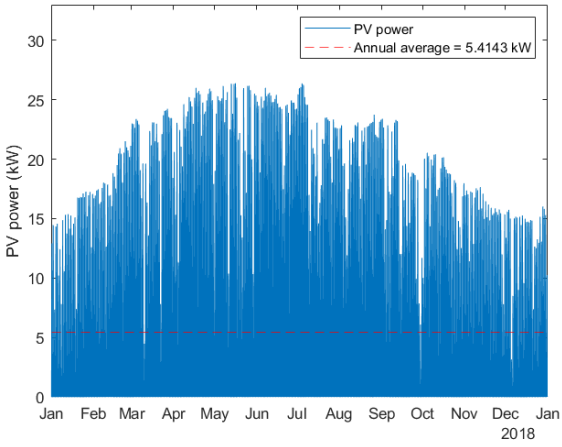

Figure 19 8760 PV production plot based on the rated PV power.

Additionally, based on the technical parameters of the chosen PV module, an initial design of the proposed PV system was performed. Here, the configuration of the proposed PV system was determined, where the maximum number of series modules and the maximum number of parallel modules were calculated based on the ambient temperature range and the short circuit capability of the inverter respectively. The equations used to determine the configuration are listed below.

The minimum number of series modules per inverter was calculated as –

$$n_{s(min)-inverter} = \frac{V_{mpp(min)-inverter}}{V_{mpp(min)-PV\ module}} \quad (18)$$

Where,

$V_{mpp(min)-inverter}$ = Minimum MPP voltage for the chosen inverter

$V_{mpp(min)-PV\ module}$ = Minimum MPP voltage for the PV module

The minimum MPP voltage for the PV module was calculated based on the highest ambient temperature seen by the vessel (obtained using the proposed data extraction technique) as shown below.

$$V_{mpp(min)-PV\ module} = V_{mpp-PVmodule} \times \left(1 + \alpha_V\left(T_{cell(max)} - 25°C\right)\right) \quad (19)$$

Where,

$V_{mpp-PVmodule}$ = Rated MPP voltage of the chosen PV module

α_V = Temperature-voltage coefficient (assumed to be -0.5% V per °C)

$T_{cell(max)}$ = Maximum cell temperature = $T_{ambient(max)} + \frac{NOCT-20°C}{0.8}$

To ensure that the maximum voltage of proposed configuration does not exceed the rated maximum DC input voltage of the inverter, the maximum number of series modules per inverter was calculated based on the calculated maximum MPP voltage and the calculated maximum open circuit voltage of the PV module as shown below.

$$n_{s(max)-inverter} = \min\left\{\frac{V_{mpp(max)-inverter}}{V_{mpp(max)-PV\ module}}, \frac{V_{dc(max)-inverter}}{V_{OC(max)-PV\ module}}\right\} \quad (20)$$

Where,

$V_{mpp(max)-inverter}$ = Maximum MPP voltage for the chosen inverter

$V_{mpp(max)-PV\ module}$= Maximum MPP voltage for the PV module

$V_{dc(max)-inverter}$ = Rated maximum DC input voltage for the chosen inverter

$V_{OC(max)-PV\ module}$ = Maximum open circuit voltage for the PV module

The maximum MPP voltage and the maximum open circuit voltage for the PV module was calculated based on the lowest ambient temperature seen by the vessel (obtained using the proposed data extraction technique) as shown below.

$$V_{mpp(max)-PV\ module} = V_{mpp-PVmodule} \times \left(1 + \alpha_V\left(T_{cell(min)} - 25°C\right)\right) \quad (21)$$

$$V_{OC(max)-PV\ module} = V_{OC-PVmodule} \times \left(1 + \alpha_V\left(T_{cell(min)} - 25°C\right)\right) \quad (22)$$

Where,

$V_{mpp-PVmodule}$ = Rated MPP voltage of the chosen PV module

$V_{OC-PVmodule}$ = Rated open circuit voltage of the chosen PV module

α_V = Temperature-voltage coefficient (assumed to be -0.5% V per °C)

$T_{cell(min)}$ = Minimum cell temperature = $T_{ambient(min)} + \frac{NOCT-20°C}{0.8}$

While calculating the maximum number of parallel modules, it was ensured that the short circuit current contribution from the PV modules does not exceed the rated short circuit withstand capability of the inverter and the maximum DC current from the PV modules does not exceed the maximum continuous DC current rating of the inverter. While calculating the maximum number of parallel modules, a factor of 1.25 was applied, per NEC Section 690.8 (A)(2), as shown below.

$$n_{p(max)-inverter} = \min\left\{\frac{I_{SC-inverter}}{1.25 \times I_{SC-PV\ module}}, \frac{I_{DC} - inverter}{I_{mpp-PV\ module}}\right\} \quad (23)$$

Where,

$I_{SC-inverter}$ = Rated DC short circuit current for the chosen inverter

$I_{SC-PV\ module}$ = Rated short circuit current for the chosen PV module

$I_{DC} - inverter$ = Rated continuous DC current for the chosen inverter

$I_{mpp-PV\ module}$ = Rated MPP current for the chosen PV module

Based on the equations listed above, the maximum number of series modules was calculated to be 14 and the maximum number of parallel modules was calculated to be 8. Therefore, the total number of PV modules is 112 thereby reducing the initial estimated DC

capacity of about 33 kW to 18.48 kW. Figure 20 illustrates the annual PV production plot based on the new estimated maximum capacity of 18.48 kW.

Table 4. Summary of costs - PV system.

Component	**Quantity**	**Per item cost**	**Total cost**
PV panel – 165 W	112	$549.99	$61,598.88
Other components			$ 3,777
Total			$65,375.88

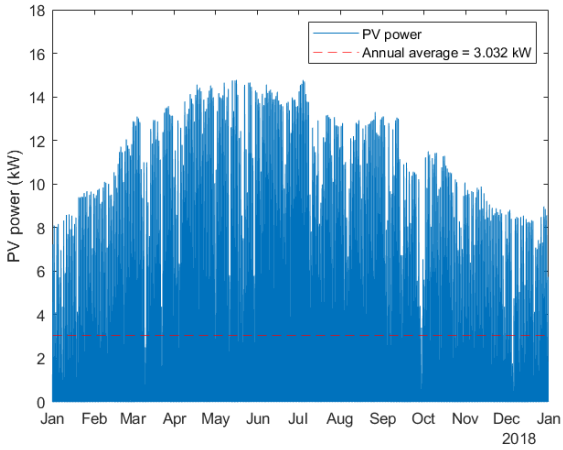

Figure 20 8760 PV production plot based on the design configuration.

4.3. Optimal scheduling of diesel generators with PV

Since this work also investigates the integration of solar PV for fuel consumption savings, an optimal dispatching scheme of the diesel generators with the proposed solar PV system has to be developed to estimate the fuel savings due to the solar PV integration.

4.3.1. Objective function

Since the overall objective of minimizing fuel consumption remains the same, the objective function is the same as the one defined in Chapter 3.

$$J = \min \sum_{t=1}^{T} \left(\sum_{n=1}^{N_{DG}} \text{fuel}(n)_t \right) \quad (24)$$

Note that the proposed work aims to study the benefits of battery storage separately from the PV. Therefore, this optimal dispatch scheme comprises of the onboard DGs and the proposed PV.

4.3.2. Constraints

Since the size of the proposed PV system small, the PV system is meant to be used for direct demand supply. Hence, the power balance constraint is defined as shown below.

$$\sum_{n=1}^{N_{DG}} P_{DG(n)_t} = P_{d_t} - P_{PV_t} \quad (25)$$

Where,

P_{PV_t} = Power produced by the solar PV system at time t

Similar to Chapter 2, since the power generated by the DG has to be a finite positive value, a DG power constraint is defined as shown below.

$$0 \leq P_{DG(n)_t} \leq U_{DG\,(n)_t} \times P_{DG}^{mx} \quad (26)$$

Also, the N-1 safety constraint is defined based on the MGO based N-1 safety calculations from Chapter 2 as shown below, where the constraint uses the vessel demand that does not include the PV power.

$$N_{DG_t}(P_{d_t}) = \begin{cases} 2, & P_{d_t} \leq 950\ \text{kW} \\ 3, & P_{d_t} > 950\ \text{kW} \end{cases} \quad (27)$$

CHAPTER 5. RESULTS AND DISCUSSION

This section presents the results obtained using the proposed optimal scheduling scheme and discusses the findings based on the results. To define the objective functions and the constraints, and to solve the proposed optimization problem, this work uses MATLAB-YALMIP [38] as the toolbox and since the objective function is quadratic, CPLEX [39] is used as the solver. The dispatch was performed on a weekly basis, and the dispatch uses the actual demand and PV power data, estimated in Chapter 2 and Chapter 4, for realisitc dispatch results.

5.1. Optimal scheduling with battery energy storage

As mentioned in the previous section, the proposed optimal scheduling scheme starts with an intial battery capacity and this value is incremented until a maximum possible value is reached, which is in turn is calculated based on the maximum allowable additional loading value, that is 48 tonnes. Since the optimal dispatching scheme accounts the round trip efficiency (RTE) of the battery, a battery chemistry has to be chosen. This work investigated the different battery chemistries that are suitable for marine applications and here is a summary of the lessons learned from the investigation –

1. Among lead acid batteries, the AGM Pb-acid (absorbed glass mat lead acid) battery is best suitable for marine vessels due to its resistance (spill, leak and vibration) qualities along with other benefits such as low self-discharge rate, long lifespan, less prone to sulfation and high depth of discharge capability. Also, flooded lead acid batteries can be used for applications that are less prone to vibrations, for example, boats that voyage in backwater environments.
2. Among lithium batteris, LFP (lithium ferrous phosphate) and NMC (nickel manganese cobalt) batteries can be used with careful battery and thermal management schemes. Their benefits over lead acid batteries include lightweight, long lifespan and energy density.

To determine the maximum possible battery capacity, weight per kWh capacity of the chosen battery is obtained from the datasheet. Table 5 summarizes the cost and weight of batteries from selected chemistries, as obtained from the vendor datasheets [40], [41]. The maximum allowable size is calculated using the battery weight per kWh value and the maximum allowable weight of 48 tonnes, and the calculated conservatively rounded down towards the nearest lower thousand value. Also, since a publicly available datasheet for marine grade NMC batteries was not found, it was assumed that the technology is 33% more expensive than LFP and the weight per kWh was conservatively assumed to be 85% of LFP [42].

Table 5. Summary of specifications for battery energy storage.

Chemistry	**Price per kWh**	**Weight per kWh**	**Maximum allowable battery size**	**RTE**
AGM Pb-acid	$ 155	23.33 kg	2000 kWh	90 %
LFP	$ 624	9.23 kg	5200 kWh	95 %
NMC	$ 830	7.84 kg	6000 kWh	95 %

Table 6 lists the values of the parameters used in the proposed optimal scheduling scheme. As indicated, the initial state of charge of the batteries is assumed to be at its minimum threshold value (SOC_{min}), since, as we know, the state of charge at the start of the year depends on the final state of charge at the end of the previous year and it was conservatively assumed that the batteries were drained to their minimum value.

Table 6. Values of constants used in the proposed optimal scheduling scheme.

Parameter	**Denotation**	**Value**
Power rating of DGs	P_{DG}^{mx}	950 kW
Maximum demand for operation of 2 DGs (N = 2)	P_{d}^{mx}	950 kW
Minimum SOC limit of battery	SOC_{min}	100 %
Maximum SOC limit of battery	SOC_{max}	10 %

Based on the values indicated in Table 5 and Table 6, the proposed optimal scheduling of DGs with a weekly horizon was executed for an entire year using MATLAB-YALMIP. As illustrated in Figure 21, for each battery chemistry, the program starts with an initial battery size of 0 kWh as a benchmark for fuel savings and increments the battery size by 500 kWh until the maximum allowable battery size, as indicated in Table 5, is reached.

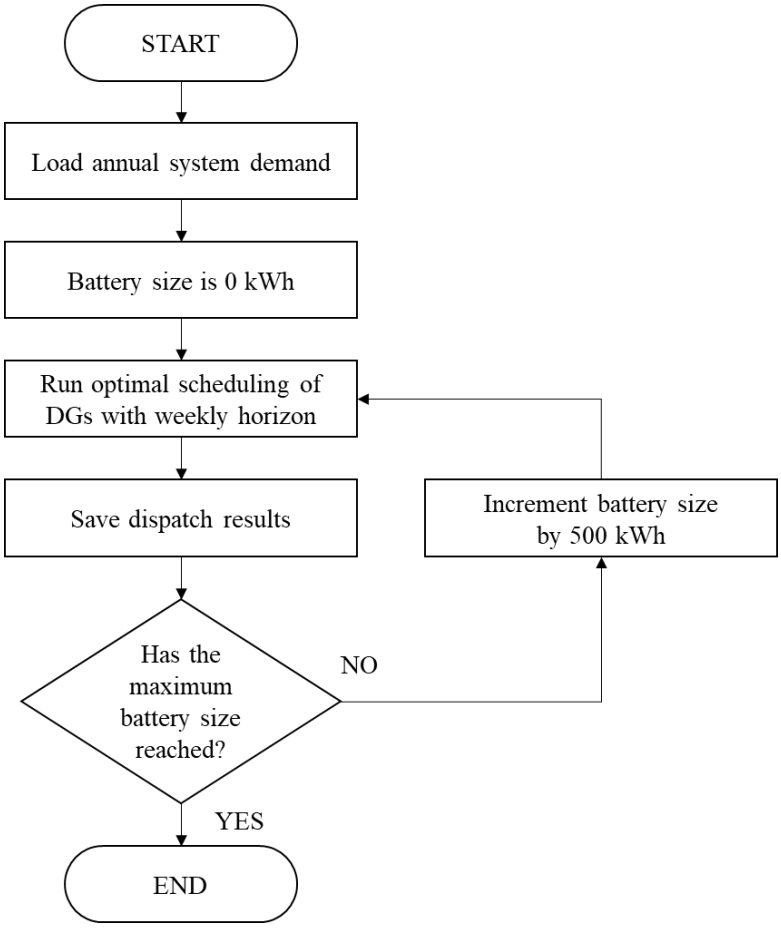

Figure 21 Battery size incrementing algorithm.

Since the power balance constraint is critical for the overall stability of the system, the first check, after obtaining the dispatch results, was to check if the optimal dispatching scheme-maintained power balance. Figure 37 illustrates a zoomed plot showing the power balance of the system. Note that the total system demand comprises of the actual vessel demand and the battery storage.

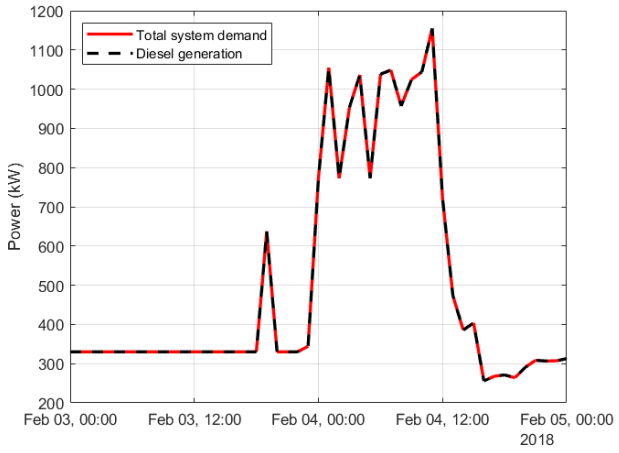

Figure 22. Zoomed plot showing power balance.

Figure 23 shows a zoomed version of the vessel demand and the battery SOC profile. Note that the figure uses the vessel demand profile to illustrate the working of the proposed optimal dispatch scheme and the vessel demand corresponds to the yearly demand profile estimated based on the ship speed and does not include the charging or discharging power of the battery. From the plots shown in Figure 23, it can be seen that whenever the system encounters a high demand condition during any given weekly horizon period, the optimal scheduling scheme charges the battery during the low demand condition and discharges the battery during the high demand condition for maximizing fuel savings. Figure 24 clearly illustrates the net positive fuel savings by charging under low demand intervals and discharging under high demand intervals.

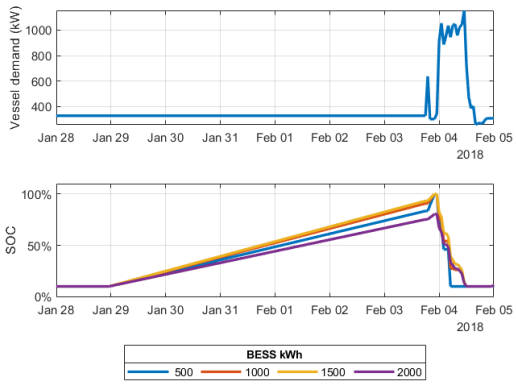

Figure 23. Zoomed vessel demand and battery SOC profile for different AGM battery sizes.

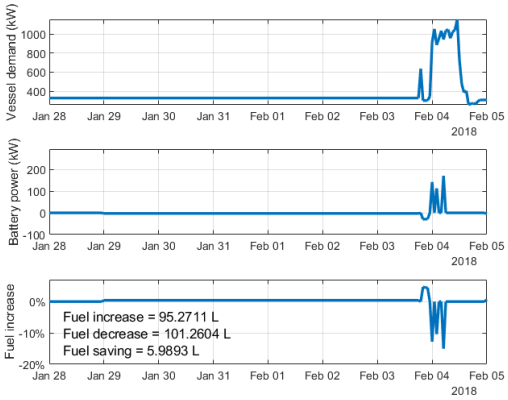

Figure 24. Zoomed vessel demand, battery power and fuel increase profile for AGM 1000kWh battery.

The working of the MGO based N-1 safety integrated into the optimal scheduling scheme is illustrated in Figure 25 using a stairstep graph. The maximum demand for 2 DGs calculated based on the minimum generator operations for N-1 safety (refer to Table 1) is marked as a red dotted line to clearly show the working of the proposed optimal scheduling scheme with MGO based N-1 safety. For example, around the midnight on February 4, the vessel demand exceeds the maximum demand for 2 DG operation. The proposed dispatching scheme responds by bringing a third generator online to comply with the MGO based N-1 safety constraint.

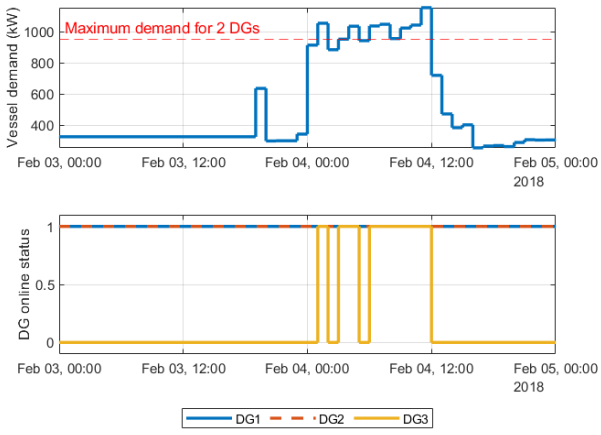

Figure 25 Zoomed vessel demand and DG online status.

Finally, for each battery size, the total annual fuel consumption by the DGs was estimated and the fuel savings from the first iteration, where the battery size was set to zero, was calculated and plotted as shown in Figure 26. Note that the fuel savings plot for AGM stops at 2000 kWh since the maximum estimated battery size for AGM chemistry is 2000 kWh. From Figure 26, it is intuitive that the amount of fuel savings achieved by a battery depends on its charging and discharging efficiencies. Since lithium-ion batteries, are more efficient than lead-acid batteries, thanks to the smaller lithium ions enabling low internal resistance, the amount of fuel savings achieved using lithium-ion batteries are much higher (almost 170 – 190%) than the fuel savings achieved using lead-acid batteries.

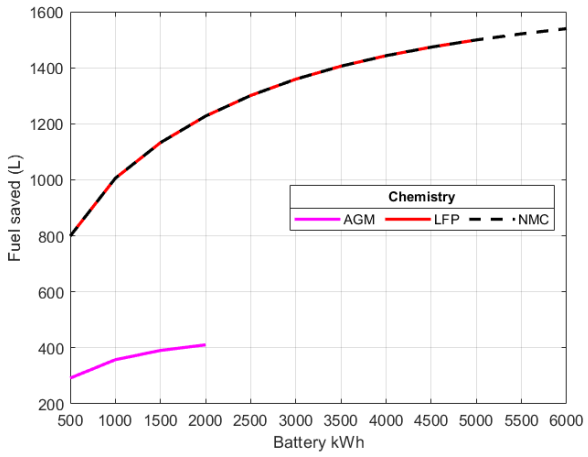

Figure 26. Fuel savings due to optimal dispatch using battery energy storage.

Also, from Figure 26 it can be seen that as the battery capacity increases, the battery is able to discharge for a longer period before being depleted, also charges less regularly, thereby, saving more fuel. However, it has to be noted that the battery discharge energy (discharge power over a time period) tends to saturate beyond a certain battery capacity since the high energy demand, that is the energy corresponding to any given high demand period, remains the same and the maximum possible fuel savings that the battery can achieve is to completely supply the high energy demand

and cannot discharge more than the vessel demand since diesel generators cannot accept power and the power balance for the system has to be maintained.

5.2. Factors that affect the fuel savings of onboard storage integration

5.2.1. Capacity degradation

Due to the gradual wearing of the internal materials used in a battery, the battery loses its capacity over time and usage. Therefore, they cannot be assumed to last forever and their lifetime needs to be accounted for an accurate study that involves comparing different battery chemistries and while evaluating the economics of the proposed system. To estimate the lifetime of the batteries chosen in this study, the number of cycles per year is estimated and it has been assumed that the usage will be the same over time.

To estimate the number of cycles per year, an equivalent full cycles estimation method [43] is used as shown in equation (28). Since the load data is for every 1 hour, although the optimization runs with a 1 week horizon, it effectively dispatches hourly, every week, for an entire year. Therefore, the time period of summation (Δt) is 1 hour.

$$Z_{yr} = \sum_{t=1}^{8760} \frac{P_d(t)}{E_{rated}} \times \Delta t \qquad (28)$$

Where,

Z_{yr} = Equivalent full cycles for 1 year

$P_d(t)$ = Discharge power at time t

E_{rated} = Energy rating of battery

Δt = Time period of summation (1 hour)

Based on the estimated equivalent full cycles for 1 year, the number of years until end of life (EOL) is estimated as shown below.

$$\mathrm{EOL_{yr}} = \frac{\mathrm{EOL_{cycles}}}{\mathrm{Z_{yr}}} \quad (29)$$

Where,

$\mathrm{EOL_{yr}}$ = Number of years until EOL

$\mathrm{EOL_{cycles}}$ = Manufacturer tested number of cycles until EOL

Here, the value for $\mathrm{EOL_{cycles}}$ is obtained from the manufacturer datasheet. Since the manufacturer might have tested the battery at a different depth of discharge (i.e., $\mathrm{EOL_{cycles(tested)}}$ at $\mathrm{DOD_{tested}}$), it has been assumed that the $\mathrm{EOL_{cycles}}$ is linearly proportional to the depth of discharge and the annual average depth of discharge, estimated using the hourly SOC values recorded by the optimal dispatch scheme, is used to estimate the corresponding $\mathrm{EOL_{corr}}$ as shown in equation (30). Also, since a publicly available manufacturer data for NMC battery was not available, it was assumed their life is 1/3rd of LFP [42].

$$\mathrm{EOL_{cycles(corr)}} = \frac{\mathrm{EOL_{cycles(tested)}} \times \mathrm{DOD_{actual}}}{\mathrm{DOD_{tested}}} \quad (30)$$

$$\therefore \mathrm{EOL_{yr}} = \frac{\mathrm{EOL_{cycles(tested)}} \times \mathrm{DOD_{actual}}}{\mathrm{DOD_{tested}} \times \mathrm{Z_{yr}}} \quad (31)$$

As shown in Figure 27 as the battery size increases, the depth of discharge increases since the dispatch scheme starts with a minimum SOC value and the larger batteries were typically discharged before reaching a fully charged state (for example, refer Figure 23). Figure 28 illustrates

the number of cycles per year estimated using (28). As expected, it can be seen that as the battery size increases, number of cycles per year decreases as the battery is subjected to less cycling.

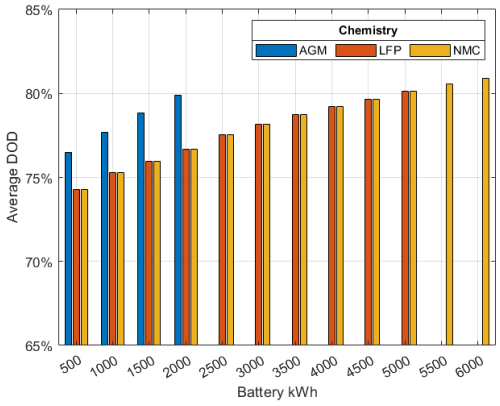

Figure 27. Annual average depth of discharge.

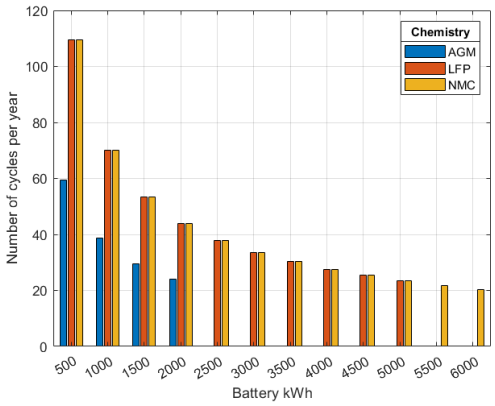

Figure 28. Equivalent number of full cycles per year.

Using the data shown in Figure 27 and Figure 28, and using equation (31), the number of years until the end of life (EOL_{yr}) is estimated and plotted as shown in Figure 29. It can be seen that the batteries are being used less frequently, therefore, have a high estimated number of years until end of life. For a conservative approach, the batteries were assumed to last a maximum of 20 years before reaching their end of life capacity. Based on this assumption, the number of years until end of life is plotted as shown in Figure 30.

Upon studing the capacity degradation of the batteries, for the vessel under study, since LFP and NMC type batteries last much longer than AGM type batteries, capacity degradation may not be a critical parameter that affects the economics of choosing a LFP battery. However, while evaluating the benefits of integrating an AGM battery for fuel savings, the capacity degradation has to be considered.

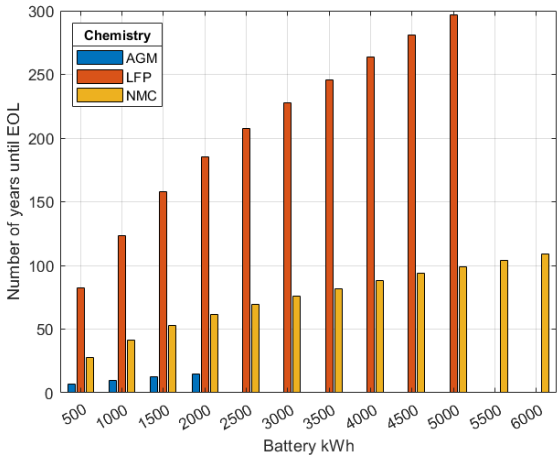

Figure 29. Number of years until end of life (EOL).

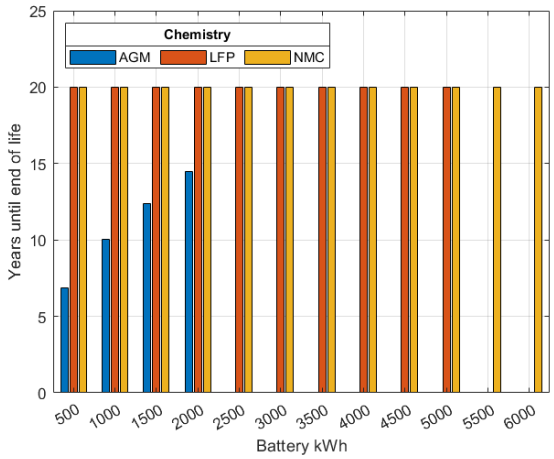

Figure 30. Number of years until end of life (EOL) with maximum lifetime of 20 years.

5.2.2. Additional weight

Since the fuel consumed by any vessel, among other factors, depends on the weight of the vessel [44], the additional weight due to the integration of battery energy storage can be considered for a more realistic fuel savings estimation. Since the amount of fuel savings estimated in the previous section does not account the additional fuel consumption due to the added weight of the storage system, this section studies the impact of the added weight of the storage system on the fuel savings.

To estimate the increase in fuel consumption due to the added weight of the storage system, a fuel correction equation is used that linearly relates the fuel consumption to the weight of the vessel [44]. Using the original fuel consumption and vessel tonnage values, the new fuel consumption value for an updated vessel tonnage can be estimated as shown below.

$$\mathrm{Fuel}_{\mathrm{new}} = \mathrm{Fuel}_{\mathrm{old}} \times \left(\frac{\mathrm{W}_{\mathrm{new}}}{\mathrm{W}_{\mathrm{old}}}\right)^{2/3} \quad (32)$$

Figure 31 illustrates the effect of considering the additional weight while estimating the fuel conusmption. Since AGM batteries are much heavier than LFP and NMC batteries, their

weight has a significant impact on the increase in fuel consumption (thereby, decrease in fuel savings), even at lower batter capacities. On an average, the additional weight of AGM batteries causes a 17 % increase in the fuel consumption, whereas the lightweight lithium-ion chemistries such as LFP and NMC cause a 15% and a 13% increase in fuel consumption, respectively.

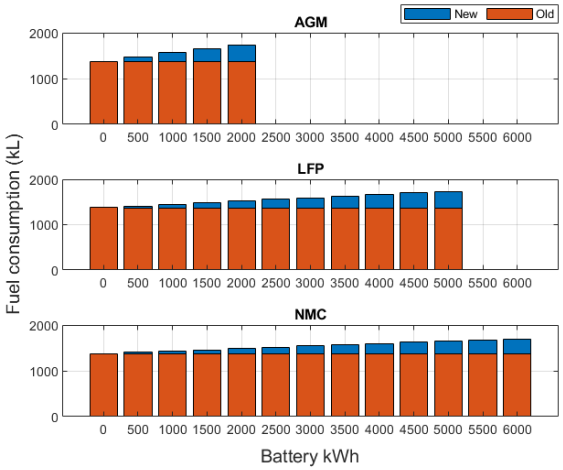

Figure 31. Fuel consumption – with (new) and without (old) weight correction.

From Figure 31, it can also be seen that the increase in the fuel consumption is much higher than the fuel savings achieved by integrating additonal battery energy storage, therefore, integrating battery energy storage might not be beneficial as far as achieving fuel savings in research vessels. Figure 32 clearly illustrates the negative benefit of integrating battery energy storage for fuel savings in the vessel under study.

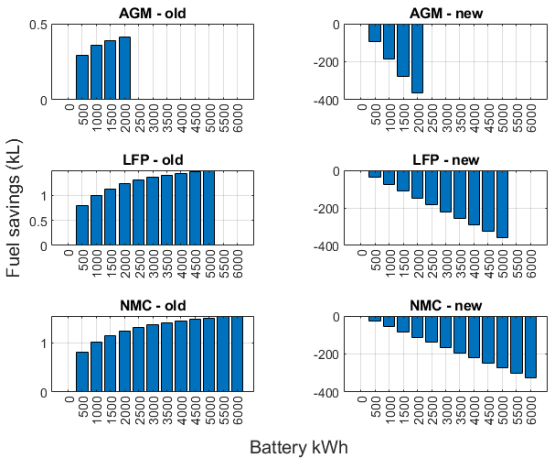

Figure 32. Fuel savings - with (new) and without (old) weight correction.

5.2.3. Load profile

While estimating the system demand based on the ship speed (refer Chapter 1), under moored condition, the vessel was assumed to consume a constant auxiliary power. In practice, the auxiliary power consumption varies based on various parameters such as the engine room temperature, vessel activity or weather conditions. Since, for the vessel under study, the data illustrating the nature of the auxiliary load variation was not available, a random varying auxiliary load data was generated as a periodic random Gaussian input signal with a period of 1 and the number of samples matching the length of the data associated with the moored operating condition. This randomized data was then normalized and the required varying auxiliary load data was obtained with an assumption that the maximum auxiliary load is 1/3rd of the maximum cruising power [31].

With the proposed optimal dispatch scheme, assuming a varying auxiliary load will have a significant effect on the achieved fuel savings, because, a constant auxiliary load will not trigger the battery operation unless the ship changes its operating condition, whereas a varying auxiliary load will continuously trigger the battery operation for maximizing fuel savings due to the mixture

of low and high demand intervals. Here, for simplicity, only AGM and LFP are considered since the fuel savings characteristics of NMC closely matches with LFP, as can be seen from Figure 26.

As illustrated in Figure 33 and Figure 34, with a varying auxiliary load, the fuel savings is significantly improved since the optimal dispatch scheme continuously charges and discharges the battery for maximizing fuel savings. As compared to the fuel savings achieved with a constant auxiliary load assumption, for the same datetime range as shown in Figure 24, with a varying auxiliary load assumption, as shown in Figure 34, the fuel savings is increased by almost 120%. From Figure 35, for a given year with a varying auxiliary load assumption, the fuel savings is increased on an average by about 50% for AGM and 32% for LFP over all possible battery sizes. Finally, Figure 36 clearly illustrates the continuous operation of the energy storage under a varying auxiliary load condition as an increase in the number of equivalent cycles per year.

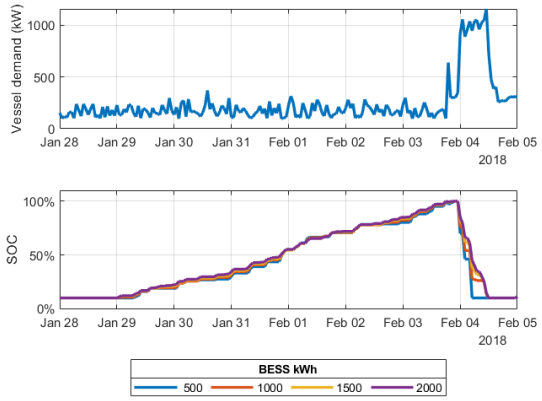

Figure 33. Zoomed varying vessel demand and battery SOC profile for different AGM battery sizes.

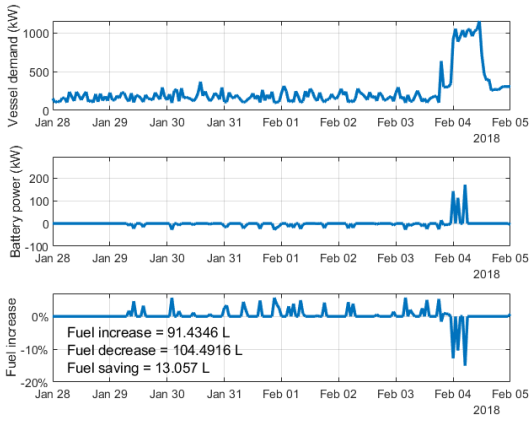

Figure 34. Zoomed varying vessel demand, battery power and fuel increase profile for AGM 1000kWh battery.

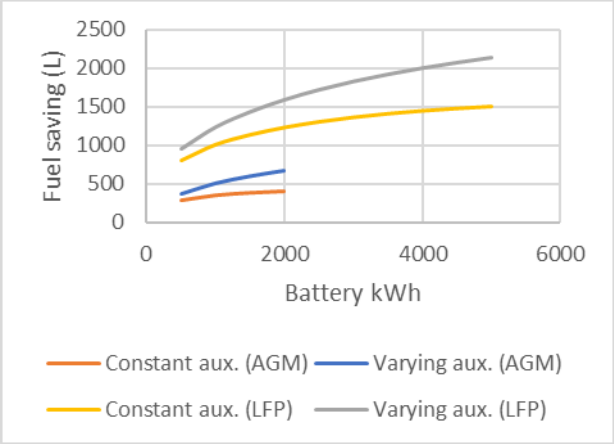

Figure 35. Annual fuel savings with varying auxiliary load.

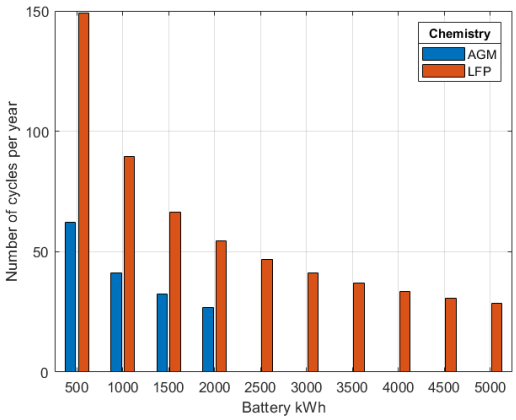

Figure 36. Equivalent number of full cycles per year with varying auxiliary load.

5.3. Optimal scheduling with PV

Using MATLAB-YALMIP, the proposed optimal dispatching scheme discussed in Chapter 4 was used to dispatch the onboard diesel generators with the proposed PV system. As mentioned previously, this work intends to study the benefits of solar PV integration separately, therefore, the demand only comprises of the vessel demand and does not include the battery energy storage system.

Since the power balance constraint is critical for the overall stability of the system, the first check, after obtaining the dispatch results, was to check if the optimal dispatching scheme-maintained power balance. Figure 37 illustrates a zoomed plot showing the power balance of the system. Note that the demand refers to the actual vessel demand.

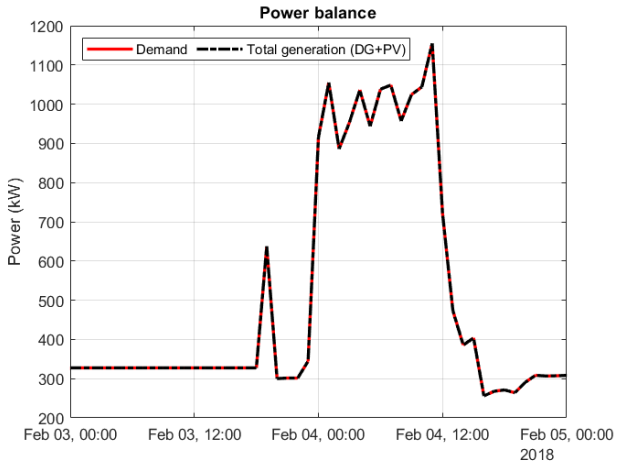

Figure 37. Zoomed power balance plot.

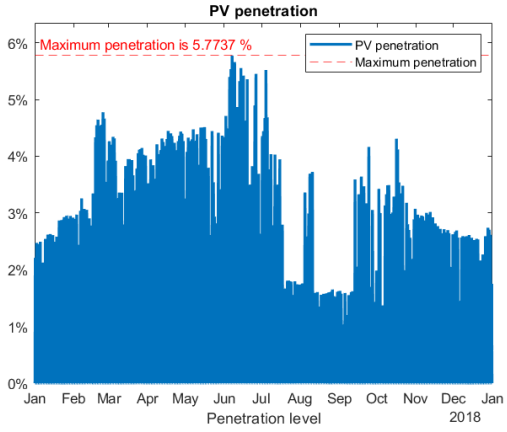

Figure 38. Annual PV penetration plot.

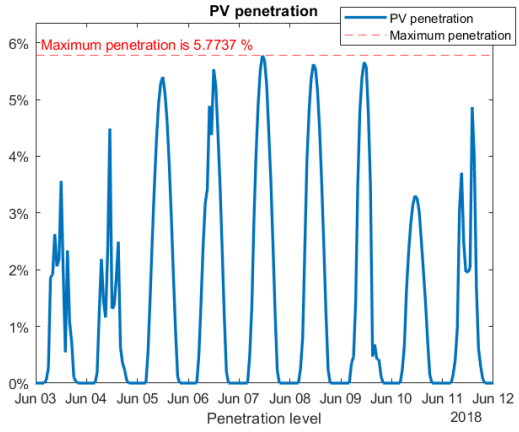

Figure 39. Zoomed PV penetration plot.

Figure 38 illustrates the annual PV penetration (ratio of PV power to the vessel demand) and Figure 39 illustrates a zoomed-in version of the annual PV penetration plot showing the region corresponding to the maximum PV penetration. As expected, the PV penetration is high during the early days of June when the vessel demand is also lower. From the zoomed-in plot shown in Figure 39, the intermittent nature of PV generation can be observed. Additional energy storage can be added to smoothen the intermittency in PV power, or the PV system can be sized larger than the PV inverters to achieve PV power clipping and additional energy storage can be used to maximize the PV benefit. These techniques are proven to be beneficial for terrestrial power systems, however, for marine power systems, due to the limited space and the impact of additional weight

on the fuel consumption, there is a very limited option for integrating additional components to the system.

Since the PV power is intermittent, its impact on the DG startup is investigated, as illustrated in Figure 40. Based on the result, the proposed the PV integration does not cause any impact on DG startup. This can be attributed to the small PV capacity and the fact that DG3 only comes online for very high demands during which the PV power is almost insignificant. Also, there are no startup values for DG1 and DG2 because, according to the MGO based N-1 safety constraint, they are always online.

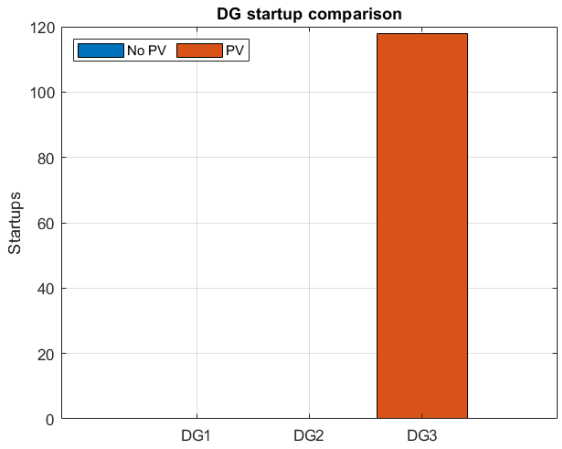

Figure 40. DG startup comparison – with and without PV.

Based on the dispatch result obtained using the optimal dispatch with and without PV, the monthly fuel consumption was estimated and plotted for comparison as shown in Figure 41. As indicated in the figure, the proposed PV system reduces the annual fuel consumption by about 5,539 liters.

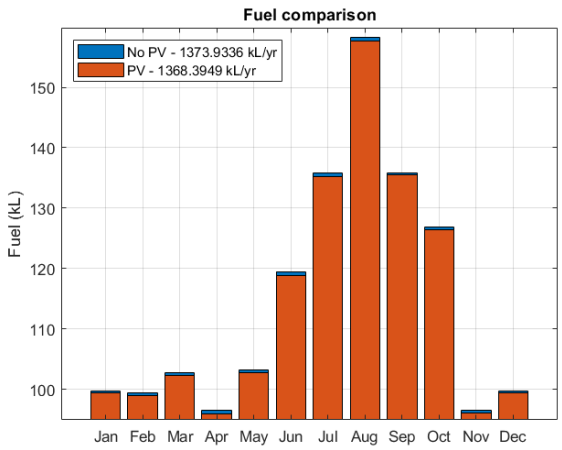

Figure 41. Fuel comparison - with and without PV.

5.4. Economic benefit through fuel savings

To evaluate the economic benefit of integrating the proposed additional PV and battery to the vessel under study, the net present value (NPV) for the proposed PV and the battery energy storage systems is calculated, as NPV is a videly used method for assesing the economic feasibilty for a system by accounting the project's revenue and expenses.

Table 7 lists the values of different parameters used to estimate the NPV for the proposed system and indicates the estimate NPV and levelized cost of energy (LCOE) values.

Table 7. Summary of economic parameters – PV system.

Attribute	**Value**
Loan principal or system cost	$65,375.88
Interest	5%
Project lifetime	25 years
Fuel saving	5538.70 liters per year
Initial fuel cost	$0.98 per liter
Fuel cost escalation rate	2% per year
Personal discount rate	10%
NPV	$ 17,828.97
Annual energy production	26,560 kWh
LCOE	$0.175/kWh

To determine the economic value of integrating PV system, the net savings per year, that is the net revenue less the costs, is calculated and plotted as shown in Figure 42. From this plot, it can be seen that, the proposed PV system starts generating revenue from the 21st year. Assuming a depreciation value of 20% the initial cost of the system, the calculated net present value of the proposed PV system is $17,828, indicating that the system is economically feasible.

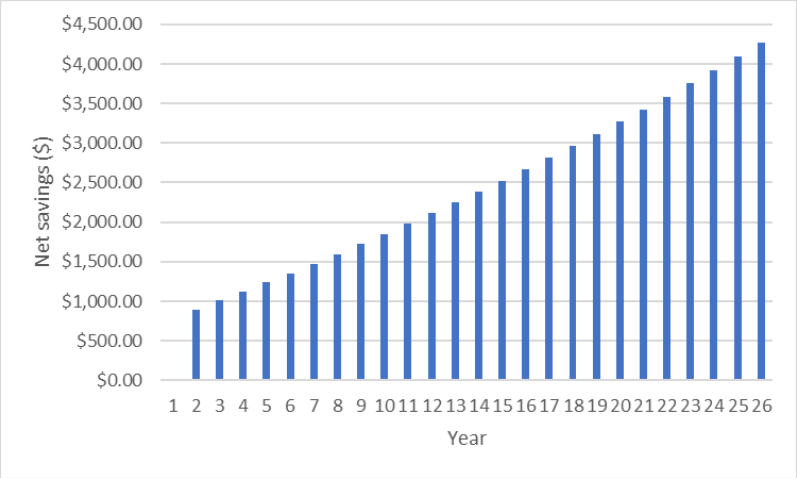

Figure 42. Net savings per year until lifetime – PV.

For the battery energy storage system, although the fuel savings was very minimal, the net present value was estimated for all the chemistries and compared as shown in Figure 43. The assumptions while estimating the NPV for the proposed battery energy storage system are listed below.

4.1.2. The different parameters that affect the fuel savings, as mentioned in 5.5.2, were not considered while calculating the NPV since considering those parameters makes the NPV even worse. With respect to the capacity degradation factor, the NPV calculation accounts the number of years until of life for project lifetime, however, does not consider the capacity degradation over time.

4.1.3. Since NMC is even more expensive than LFP, the NPV calculation for NMC is not shown in the comparison.

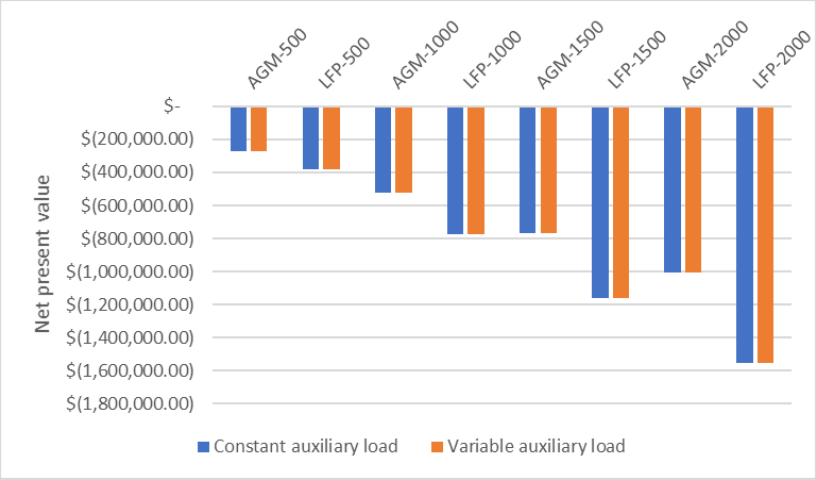

Figure 43. NPV comparison – battery energy storage.

Based on the NPV calculation, integrating battery energy storage for the vessel under study might not be economically feasible. Therefore, NPV may not be the best parameter to determine the optimal battery size.

5.5. Emission savings

For vessels similar to the vessel under study, the emissions can be calculated directly using the fuel consumption [45]. Therefore, fuel savings directly tranlsate to savings in emissions. However, the potential emission savings might be reduced by the DG startups. Therefore, the number of startups with the battery storage was estimated and was found to be low for an entire year which indicated that the startups will not signifcantly impact the emission savings.

The amount of emission savings with the proposed PV and battery energy storage system is estimated based on the emission factors obtained from the US enivornmental protection agency (EPA) emission factor data [46] as indicated in Table 8. Since mordern diesel engines use NO_x reduction catalysts, the majority of the diesel fuel combustion includes CO_2 emissions. Figure 44 and Figure 45 illustrates the emission savings in tonnes per year due to the proposed PV system and the battery systems respectively.

Table 8. US EPA emission factors for marine diesel fuel combustion.

Emitted pollutant	**Emission factor**
CO2	10.2 kg per gallon
CH4	0.00006 kg per gallon
NO2	0.00045 kg per gallon

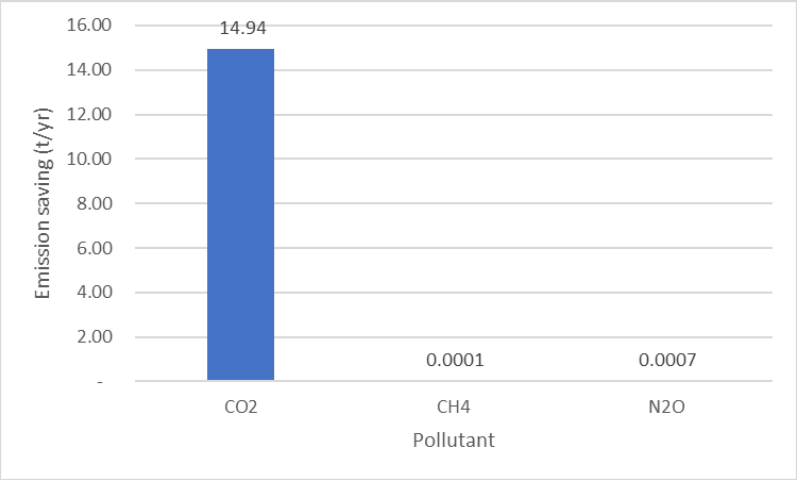

Figure 44. Emission savings due to PV integration.

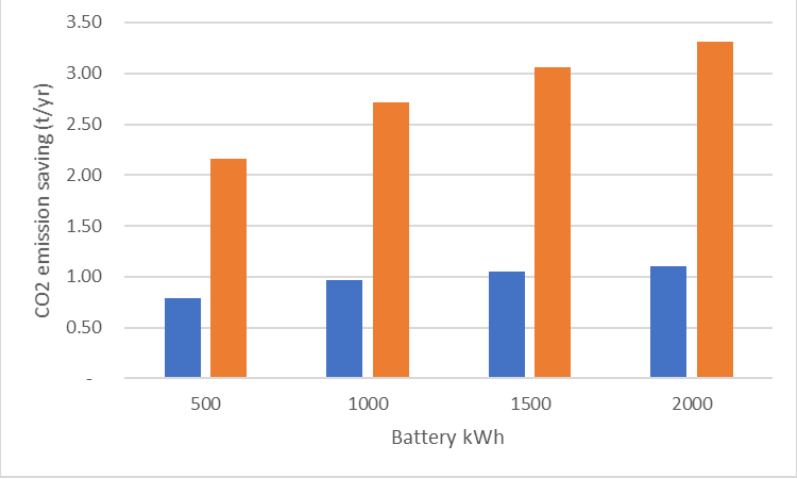

Figure 45. Emission savings due to BESS integration.

5.6. Sizing of battery energy storage system

As found in the previous section, the integration of the proposed energy storage system did not seem economically feasible, therefore, an optimal battery size cannot be determined using the NPV of the storage system. Therefore, the amount of emission savings with the proposed energy storage system was estimated and a cost to benefit ratio was determined for AGM and LFP battteries (since NMC is much more expensive than LFP) to determine the optimal battery size. This cost to benefit ratio was calculated as the ratio of the total cost of the battery energy storage system to the amount of savings in CO_2 emissions over the entire system lifetime (estimated as shown in Figure 30). As shown in Figure 46, LFP batteries have much lower cost to emission savings ratio as compared to AGM batteries. This can be attributed to their longer lifetime values and the higher achieved fuel savings. Therefore, based on the cost to emission savings ratio, a 500kWh LFP battery might be the optimal size, as larger LFP batteries did not yield significantly lower cost to emission savings ratios.

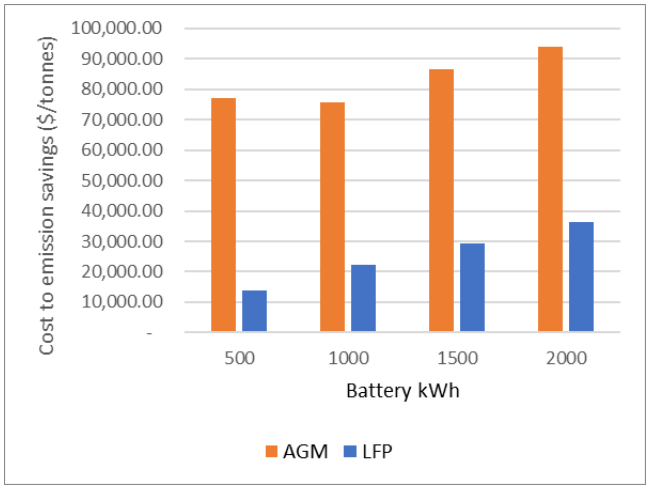

Figure 46. Battery system cost to savings in emissions ratio.

CHAPTER 7. CONCLUSION

This work started with a literature review of the studies that investigated the integration of renewable energy resources to marine vessels and proposed an optimal dispatch of those resources for fuel savings. Based on the review, it was found that a comprehensive study that uses a real-time data and the N-1 safety to optimally dispatch the onboard resources and quantify the achieved fuel and emission savings by also discussing the economics of the proposed system was missing. Therefore, this work aimed at providing a comprehensive realistic investigation of integrating renewable resources to a marine vessel. For a realistic investigation, this work estimated the real-time demand for the vessel under study and estimated the PV power production using an accurate irradiation and temperature data extraction algorithm. The optimal dispatching scheme for fuel savings used the estimated real-time data for realistic dispatch of the onboard generation and storage resources by considering the standard set of constraints but also considering the minimum generator operation with the N-1 safety constraint. To investigate the benefits of PV and BESS integration individually, separate optimal dispatching results were obtained and discussed. The observations from the dispatch results for PV and battery storage are summarized individually.

Battery energy storage –

1. The benefits of battery storage integration were observed to be closely aligning with the nature of the demand profile and the round-trip efficiency of the battery.
2. For vessels that are predominantly moored or docked, like the vessel used as the case study in this work, the storage integration might not be economically beneficial due to the minimum overall share of high demand intervals.
3. To determine the optimal battery storage size in such vessels where economic indicators such as NPV might not work, cost to emission savings can be used.

4. There is also an observed tradeoff between safety, investment cost and achieved fuel savings. Using lithium-ion batteries shall yield higher fuel savings than lead acid batteries due to their higher round trip efficiency, however, they can easily catch fire leading to the requirement for careful thermal management systems and are more expensive. On the other hand, AGM batteries are safer and cheaper but have much lower round trip efficiency than the lithium-ion batteries, therefore, yielding lower fuel savings.

PV –

1. The benefits closely aligned with the available surface area and the route taken by a marine vessel, since that would determine the solar irradiation and the ambient temperature.
2. The sizing of a marine PV system mainly depends on the available non-commercial surface area and for systems that allow integration of large-scale PV systems need to consider PV power smoothing techniques for power quality.

Finally, based on the observations, for vessels similar to the one chosen in this study, integration of a PV system might be more beneficial in terms of cost to emissions savings as compared to a battery storage system unless the battery storage systems become more feasible. However, with alternate storage technologies such as fuel cells also gaining more popularity, future works can also investigate alternate storage technologies and can perform a comparison between different storage technologies. Also, the storage fuel savings factors discussed in this work discussed can also be considered by future works for a more realistic economic evaluation and in addition to the weight limitation, the space constraint for the storage can also be accounted.

REFERENCES

[1] T. Carlo and Riccardo De Lauretis, “EMEP/EEA air pollutant emission inventory guidebook 2019,” 2020.

[2] D. P. P. Dr. Jasper Faber, Shinichi Hanayama, Dr. Shuang Zhang, “Fourth IMO GHG Study 2020,” 2021.

[3] M. James J. Corbett, James J. Winebrake, Edward W. Carr, Jukka-Pekka Jalkanen, Lasse Johansson, Marje Prank and Sofiev, “Study on effects of the entry into force of the global 0.5% fuel oil sulphur content limit on human health,” 2016.

[4] “Amendments to the 2018 guidelines on the method of calculation of the attained energy efficiency design index (EEDI) for new ships.”

[5] T. Breivik *et al.*, “Future Ship Powering Options – exploring alternative methods of ship propulsion.” [Online]. Available: https://wwwcdn.imo.org/localresources/en/OurWork/Environment/Documents/Air pollution/Future_ship_powering_options_report.pdf.

[6] E. Skjong, R. Volden, E. Rodskar, M. Molinas, T. A. Johansen, and J. Cunningham, “Past, present, and future challenges of the marine vessel’s electrical power system,” *IEEE Trans. Transp. Electrif.*, vol. 2, no. 4, pp. 522–537, 2016, doi: 10.1109/TTE.2016.2552720.

[7] M. L. Alf Kåre Ådnanes, “Autonomy requires fault tolerant, reconfigurable and connected electrical grid for propulsion,” 2019. https://new.abb.com/news/detail/24670/autonomy-requires-fault-tolerant-reconfigurable-and-connected-electrical-grid-for-propulsion (accessed Jun. 16, 2021).

[8] M. U. Mutarraf, Y. Terriche, K. A. K. Niazi, J. C. Vasquez, and J. M. Guerrero, *Energy storage systems for shipboard microgrids—A review*, vol. 11, no. 12. 2018.

[9] J. M. Guerrero *et al.*, "Shipboard microgrids: maritime islanded power systems technologies," *PCIM Asia 2016 - Int. Exhib. Conf. Power Electron. Intell. Motion, Renew. Energy Energy Manag.*, no. June, pp. 28–30, 2016.

[10] C. Nuchturee, T. Li, and H. Xia, "Energy efficiency of integrated electric propulsion for ships – A review," *Renew. Sustain. Energy Rev.*, vol. 134, no. July, 2020, doi: 10.1016/j.rser.2020.110145.

[11] M. U. Mutarraf, Y. Terriche, K. A. Khan Niazi, C. L. Su, J. C. Vasquez, and J. M. Guerrero, "Battery Energy Storage Systems for Mitigating Fluctuations Caused by Pulse Loads and Propulsion Motors in Shipboard Microgrids," *IEEE Int. Symp. Ind. Electron.*, vol. 2019-June, pp. 1047–1052, 2019, doi: 10.1109/ISIE.2019.8781182.

[12] K. Satpathi, A. Ukil, S. S. Nag, J. Pou, and M. A. Zagrodnik, "DC Marine Power System: Transient Behavior and Fault Management Aspects," *IEEE Trans. Ind. Informatics*, vol. 15, no. 4, pp. 1911–1925, 2019, doi: 10.1109/TII.2018.2864598.

[13] J. O. Lindtjørn, "Onboard DC Grid – a system platform at the heart of Shipping 4 . 0," no. October, pp. 160–167, 2017.

[14] J. A. Momoh, S. S. Kaddah, and W. Salawu, "Security assessment of DC zonal naval-ship power system," *LESCOPE 2001 - 2001 Large Eng. Syst. Conf. Power Eng. Powering Beyond 2001, Conf. Proc.*, pp. 206–212, 2001, doi: 10.1109/LESCPE.2001.941652.

[15] K. Kim, K. Park, G. Roh, and K. Chun, "DC-grid system for ships: a study of benefits and technical considerations," *J. Int. Marit. Safety, Environ. Aff. Shipp.*, vol. 2, no. 1, pp. 1–12, 2018, doi: 10.1080/25725084.2018.1490239.

[16] F. D. Kanellos, G. J. Tsekouras, and J. Prousalidis, "Onboard DC grid employing smart grid technology: Challenges, state of the art and future prospects," *IET Electr. Syst. Transp.*, vol.

5, no. 1, pp. 1–11, 2015, doi: 10.1049/iet-est.2013.0056.

[17] K. Satpathi, V. S. K. M. Balijepalli, and A. Ukil, “Modeling and Real-Time Scheduling of DC Platform Supply Vessel for Fuel Efficient Operation,” *IEEE Trans. Transp. Electrif.*, vol. 3, no. 3, pp. 762–778, 2017, doi: 10.1109/TTE.2017.2744180.

[18] I. S. C. C. 21, *IEEE Recommended Practice for Sizing Lead-Acid Batteries for Photovoltaic (PV) Systems*, vol. 2000, no. July. 2000.

[19] IEEE, *IEEE 1562-2007 Guide for Array and Battery Sizing in Stand-Alone Photovoltaic (PV) Systems*, no. May. 2008.

[20] MTU, “Technical Project Guide Marine Application,” 2008.

[21] IEEE std.45.5 - 2014, *IEEE Recommended Practice for Electrical Installations on Shipboard— Design*. 2015.

[22] S. H. Kim, M. Il Roh, M. J. Oh, S. W. Park, and I. Il Kim, “Estimation of ship operational efficiency from AIS data using big data technology,” *Int. J. Nav. Archit. Ocean Eng.*, vol. 12, pp. 440–454, 2020, doi: 10.1016/j.ijnaoe.2020.03.007.

[23] G. L. Se, “Rules for Classification and Construction Ship Technology,” 2013.

[24] S. Solem, K. Fagerholt, S. O. Erikstad, and Ø. Patricksson, “Optimization of diesel electric machinery system configuration in conceptual ship design,” *J. Mar. Sci. Technol.*, vol. 20, no. 3, pp. 406–416, 2015, doi: 10.1007/s00773-015-0307-4.

[25] F. Diab, H. Lan, and S. Ali, “Novel comparison study between the hybrid renewable energy systems on land and on ship,” *Renew. Sustain. Energy Rev.*, vol. 63, pp. 452–463, 2016, doi: 10.1016/j.rser.2016.05.053.

[26] IEEE std.45.5 - 2014, *IEEE Recommended Practice for Electrical Installations on Shipboard— Safety Considerations*. 2015.

[27] H. Lan, S. Wen, Y. Y. Hong, D. C. Yu, and L. Zhang, "Optimal sizing of hybrid PV/diesel/battery in ship power system," *Appl. Energy*, vol. 158, pp. 26–34, 2015, doi: 10.1016/j.apenergy.2015.08.031.

[28] Y. Qiu, C. Yuan, J. Tang, and X. Tang, "Techno-economic analysis of PV systems integrated into ship power grid: A case study," *Energy Convers. Manag.*, vol. 198, no. August, p. 111925, 2019, doi: 10.1016/j.enconman.2019.111925.

[29] S. Kim, S. Choe, S. Ko, and S. Sul, "A Naval Integrated Power System with a Battery Energy Storage System: : Fuel efficiency, reliability, and quality of power," *IEEE Electrif. Mag.*, no. May, pp. 22–33, 2015.

[30] M. R. Banaei and R. Alizadeh, "Simulation-Based Modeling and Power Management of All-Electric Ships Based on Renewable Energy Generation Using Model Predictive Control Strategy," *IEEE Intell. Transp. Syst. Mag.*, vol. 8, no. 2, pp. 90–103, 2016, doi: 10.1109/MITS.2016.2533960.

[31] E. Skjong, T. A. Johansen, M. Molinas, and A. J. Sorensen, "Approaches to Economic Energy Management in Diesel-Electric Marine Vessels," *IEEE Trans. Transp. Electrif.*, vol. 3, no. 1, pp. 22–35, 2017, doi: 10.1109/TTE.2017.2648178.

[32] G. Seenumani, "Real-time power management of hybrid power systems in all electric ship applications," *ProQuest Diss. Theses*, vol. 3429396, p. 151, 2010.

[33] F. D. Kanellos, "Optimal power management with GHG emissions limitation in all-electric ship power systems comprising energy storage systems," *IEEE Trans. Power Syst.*, vol. 29, no. 1, pp. 330–339, 2014, doi: 10.1109/TPWRS.2013.2280064.

[34] B. Zahedi, L. E. Norum, and K. B. Ludvigsen, "Optimized efficiency of all-electric ships by dc hybrid power systems," *J. Power Sources*, vol. 255, pp. 341–354, 2014, doi:

10.1016/j.jpowsour.2014.01.031.

[35] F. D. Kanellos, G. J. Tsekouras, and N. D. Hatziargyriou, "Optimal demand-side management and power generation scheduling in an all-electric ship," *IEEE Trans. Sustain. Energy*, vol. 5, no. 4, pp. 1166–1175, 2014, doi: 10.1109/TSTE.2014.2336973.

[36] F. Meng, C. Zhang, and Y. Zhao, "Modeling and simulation of marine propeller load," *2016 IEEE Int. Conf. Mechatronics Autom. IEEE ICMA 2016*, vol. 0, no. 5, pp. 2371–2375, 2016, doi: 10.1109/ICMA.2016.7558936.

[37] "Approximate Diesel Fuel Consumption Chart," *Generator Source*. https://www.generatorsource.com/Diesel_Fuel_Consumption.aspx.

[38] J. Löfberg, "YALMIP: A toolbox for modeling and optimization in MATLAB," *Proc. IEEE Int. Symp. Comput. Control Syst. Des.*, pp. 284–289, 2004, doi: 10.1109/cacsd.2004.1393890.

[39] IBM, "V12.10: User's Manual for CPLEX," 2019.

[40] Renogy, "Deep Cycle AGM Battery 12 Volt 200Ah," *RNG-BATT-AGM12-200-US datasheet*, 2020. https://store-fhnch.mybigcommerce.com/content/RNG-BATT-AGM12-200/AGM200-Datasheet.pdf.

[41] Renogy, "12V 100Ah Smart Lithium Iron Phosphate Battery," *RBT100LFP12S datasheet*, 2019. https://store-fhnch.mybigcommerce.com/content/RBT100LFP12S-G1/LFP100S-Datasheet.pdf.

[42] Nickel Institute, "Battle of the batteries - Cost versus Performance," 2020. https://nickelinstitute.org/blog/2020/june/battle-of-the-batteries-cost-versus-performance/.

[43] and J. L. B.-A. R. Dufo-López, T. Cortés-Arcos, J. S. Artal-Sevil, "Comparison of Lead-Acid and Li-Ion Batteries Lifetime Prediction Models in Stand-Alone Photovoltaic

Systems," *Appl. Sci.*, vol. 11, no. 3, p. 1099, 2021.

[44] N. Bialystocki and D. Konovessis, "On the estimation of ship ' s fuel consumption and speed curve : A statistical approach," *J. Ocean Eng. Sci.*, vol. 1, no. 2, pp. 157–166, 2016, doi: 10.1016/j.joes.2016.02.001.

[45] J. Coello, I. Williams, D. A. Hudson, and S. Kemp, "An AIS-based approach to calculate atmospheric emissions from the UK fishing fleet," *Atmos. Environ.*, vol. 114, pp. 1–7, 2015, doi: 10.1016/j.atmosenv.2015.05.011.

[46] US EPA, "Emission Factors for Greenhouse Gas Inventories," 2018. https://www.epa.gov/sites/default/files/2018-03/documents/emission-factors_mar_2018_0.pdf.